

Blast-induced liquefaction in silty sands for full-scale testing of ground improvement methods: Insights from a multidisciplinary study

Sara Amoroso^{a,b,*}, Kyle M. Rollins^c, Paul Andersen^c, Guido Gottardi^d, Laura Tonni^d, Maria F. García Martínez^d, Kord Wissmann^e, Luca Minarelli^b, Cesare Comina^f, Daniela Fontana^g, Paolo Marco De Martini^h, Paola Monacoⁱ, Arianna Pesci^j, Vincenzo Sapia^h, Maurizio Vassallo^b, Marco Anzidei^h, Andrea Carpena^k, Francesca Cinti^h, Riccardo Civico^h, Iginò Coco^h, Dario Conforti^l, Fawzi Doumaz^h, Fabio Giannattasio^h, Giuseppe Di Giulio^b, Sebastiano Foti^m, Fabiana Loddo^j, Stefano Lugli^g, Maria R. Manuelⁿ, Diego Marchetti^o, Mauro Mariotti^p, Valerio Materni^h, Brian Metcalfe^e, Giuliano Milana^h, Daniela Pantosti^h, Antonio Pesce^f, Aura C. Salocchi^g, Alessandra Smedile^h, Marco Stefani^q, Gabriele Tarabusi^j, Giordano Teza^r

^a Department of Engineering and Geology, University of Chieti-Pescara, Viale Pindaro 42, 65129 Pescara, Italy

^b Istituto Nazionale di Geofisica e Vulcanologia, viale Crispi 43, 67100 L'Aquila, Italy

^c Department of Civil and Environmental Engineering, Brigham Young University, 430 Engineering Building, Provo, UT 84602, USA

^d Department of Civil, Chemical, Environmental, and Materials Engineering, University of Bologna, Viale del Risorgimento 2, 40136 Bologna, Italy

^e Geopier Foundation Company, 130 Harbour Place Drive, Davidson, NC 28036, USA

^f Department of Earth Sciences, University of Turin, via Valperga Caluso 35, 10125 Torino, Italy

^g Department of Chemical and Geological Sciences, University of Modena and Reggio Emilia, via Campi 103, 41125 Modena, Italy

^h Istituto Nazionale di Geofisica e Vulcanologia, via di Vigna Murata 605, 00143 Rome, Italy

ⁱ Department of Civil, Construction-Architectural and Environmental Engineering, University of L'Aquila, Piazzale Ernesto Pontieri, Monteluco di Roio, 67100 L'Aquila, Italy

^j Istituto Nazionale di Geofisica e Vulcanologia, via Donato Creti 12, 40128 Bologna, Italy

^k Georeflex srl, via Carlo Fioruzzi 15, 29121 Piacenza, Italy

^l Teledyne Optech Incorporated, 300 Interchange Way, Vaughan, ON L4K 5Z8, Canada

^m Department of Structural, Building and Geotechnical Engineering, Politecnico di Torino, corso Duca degli Abruzzi 24, 10129 Turin, Italy

ⁿ GEO Geotecnica e Geognostica Srl, Via Faucio 16, 03033 Arpino, Italy

^o Studio Prof. Marchetti Srl, via Bracciano 38, 00189 Rome, Italy

^p Sara Electronic Instruments Srl, Via A. Mercuri 4, 06129 Perugia, Italy

^q Department of Architecture, University of Ferrara, Via della Ghiara 36, 44121 Ferrara, Italy

^r Department of Geosciences, University of Padua, via Gradenigo 6, 35131 Padua, Italy

ARTICLE INFO

Keywords:

Liquefaction

Blast test

Rammed aggregate piers

Ground improvement

Silty sands

Emilia-Romagna earthquake

ABSTRACT

In the engineering geology field increased attention has been posed in recent years to potential liquefaction mitigation interventions in susceptible sand formations. In silty sands this is a major challenge because, as the fines content increases, vibratory methods for densification become progressively less effective. An alternative mitigation technique can be the installation of Rammed Aggregate Pier® (RAP) columns that can increase the resistance of the soil, accounting for its lateral stress increase and for the stiffness increase from soil and RAP composite response. To investigate the influence of these factors on liquefaction resistance, full-scale blast tests were performed at a silty sand site in Bondeno (Ferrara, Italy) where liquefaction was observed after the 2012 Emilia-Romagna earthquake. A multidisciplinary team of forty researchers carried out devoted experimental activities aimed at better understanding the liquefaction process at the field scale and the effectiveness of the treatment using inter-related methods. Both natural and improved areas were investigated by in-situ tests and later subjected to controlled blasting. The blast tests were monitored with geotechnical and geophysical instrumentation, topographical surveying and geological analyses on the sand boils. Results showed the RAP effectiveness due to the improvement of soil properties within the liquefiable layer and a consequent reduction of the blast-induced liquefaction settlements, likely due to soil densification and increased lateral stress. The applied multidisciplinary approach adopted for the study allowed better understanding of the mechanism

* Corresponding author at: Department of Engineering and Geology, University of Chieti-Pescara, Viale Pindaro 42, 65129 Pescara, Italy
E-mail address: sara.amoroso@unich.it (S. Amoroso).

involved in the liquefaction mitigation intervention and provided a better overall evaluation of mitigation effectiveness.

1. Introduction

The identification of an effective soil improvement technique for the mitigation of liquefaction hazard in silty sand deposits is undoubtedly a major challenge for engineers, geologists, building owners, developers, and specialty contractors. Indeed, as the fines content increases, the normally adopted vibratory methods for densification become progressively less effective and therefore more expensive approaches, such as soil mixing or deep foundations, are often required. Most of these alternative techniques are based on the installation of stiffer elements within the soil aimed at increasing both strength and soil density: typical examples are the Rammed Aggregate Piers® (RAP), Stone Columns (SC), Low Mobility Grout (LMG) or Timber Displacement Pile (TDP). In recent years, the Resonant Compaction Method (RCM) has also been investigated as a ground improvement solution in liquefaction-prone silts-silty sands (e.g. Li et al., 2018).

Over the last decades, a large amount of research has been carried out on liquefaction mitigation in clean sands, especially with reference to ground improvement techniques by densification. In recent years research interest has been also extended to liquefaction-prone deposits of silts and silty sands. It is worth mentioning here the valuable outcomes from the extensive investigations carried out in Christchurch (New Zealand), following the widespread liquefaction and lateral spreading evidences due to the 2010–2011 Canterbury earthquake sequence (Giona Bucci et al., 2018). Wissmann et al. (2015), Vautherin et al. (2017), and Amoroso et al. (2018) examined the performance of RAP installation, showing that densification can be obtained and reliably quantified by means of piezocone (CPTU) and flat dilatometer (DMT) measurements in granular soil deposits having a soil behaviour type index $I_c < 1.8$ or a material index $I_D > 1.8$, also at depths exceeding the design treatment depth. Wotherspoon et al. (2015) and Hwang et al. (2017) assessed the effectiveness of soil stiffening caused by the installation of SC, RAP and LMG using cross-hole tests. RAP appeared to produce stiffer discrete inclusions than SC, while LMG column installation actually compromised the liquefaction resistance. Finally, Alexander et al. (2017) examined the performance of a SC foundation system subjected to the Canterbury earthquake, showing that SC can cause contamination of gravel with silty fines and prevent drainage during shaking, thus resulting in loss of performance.

After the 1989 Loma Prieta earthquake, mitigation strategies against liquefaction in silty sands were also analyzed by Mitchell and Wentz (1991), who compared the performance of sites reinforced by SC with that of adjacent untreated areas. Minor or negligible damage was observed in the improved soils, whereas cracks and/or settlements, primarily due to liquefaction, occurred in untreated soil deposits. However, as the non-plastic fines content increased, the SC technique appeared to be more successful in combination with pre-installed wick drains (Adalier et al., 2003). Gianella and Stuedlein (2017) studied the behavior of sands and silty sands treated by TDP in South Carolina, proposing this technique as a suitable and potentially sustainable ground improvement alternative. Significant increases in cone resistance were observed after installation, though followed by a reduction in the long term. Finally, Li et al. (2018) reported a series of in-situ tests and full-scale field tests to investigate the RCM compaction effects on laterally loaded piles in silts and silty sands in eastern China, showing that this approach results in increase lateral resistance of the piles as well as in a reduction in soil liquefaction potential.

The increase in penetration resistance due to the installation of the ground improvement techniques described previously is generally attributed to the increase in soil density alone, erroneously neglecting the influence of lateral stress. Nonetheless, it has been observed (Harada

et al., 2010; Salgado et al., 1997) that the potential increment of lateral pressure can go well above the normally-consolidated state, thus contributing to the increase of the liquefaction resistance within the improved soils. In addition, it is still uncertain how to accurately account for the composite action of discrete elements and soil. Soil-cement columns or grids constructed by cement deep soil mixing, jet grouting, or other methods (e.g. SC) are considered effective for mitigating liquefaction in silty sands by shear reinforcement mechanism (e.g. Mitchell, 2008; Adalier and Elgamal, 2004). However, recent numerical studies by Rayamajhi et al. (2014, 2016) and Green et al. (2008) demonstrated that discrete columns may deform in both flexure and shear, being less effective in reducing shear stresses than what shear stress compatibility implies. Investigations based on vibroseis “T-Rex” and/or cross-hole tests in New Zealand and Ecuador (Wissmann et al., 2015; Smith and Wissmann, 2018) provided evidence that RAP reinforced ground is significantly stiffer than the untreated natural soil.

The level of shear stress reduction in the surrounding soil due to the in-situ installation of discrete columns has still not been demonstrated by field data. Therefore, full-scale liquefaction tests in the field, under controlled conditions, are important for a proper quantification of lateral stress and shear stiffening phenomena. These tests will improve understanding of the behavior of the soil and column composite response under conditions similar to those induced by earthquakes.

Previous experiences in the United States and New Zealand (e.g. Ashford et al., 2004; Wentz et al., 2015; Saftner et al., 2015; Gianella and Stuedlein, 2017) show that liquefaction can be induced and monitored in clean sands with controlled blasting. Some efforts have also recently focused on studying the behavior of siltier deposits during blast-liquefaction tests in Italy (Amoroso et al., 2017; Fontana et al., 2019; Passeri et al., 2018; Pesci et al., 2018). Furthermore, little research is available to demonstrate RAP effectiveness in mitigating liquefaction in sandy silts and silty sands, using blast-induced liquefaction. Nevertheless, preliminary results from a silty sandy case history in Ecuador suggest that RAP ground improvement elements installed beneath a 700 m-long bridge embankment prevented lateral spreading and settlement during the 2016, M_w 7.8 Muisne earthquake (Smith and Wissmann, 2018).

In this context, full-scale blast tests were performed at a silty sand site in Bondeno (Ferrara, Italy) where liquefaction was observed after the 2012 Emilia-Romagna earthquake (Emergeo Working Group, 2013), as preliminarily presented by Amoroso et al. (2019). Compared to previous blast experiences, the present study is based on a multi-disciplinary approach, involving a team of forty researchers with expertise in the fields of geology, geophysics, geotechnical engineering and site surveying, in order to gain a comprehensive understanding of the mechanisms governing the selected engineering solution for liquefaction mitigation. Geotechnical testing, surface seismic and geoelectrical surveys were performed before and after RAP installation, as well as after blasting, to verify the effectiveness of the treatment. An array of explosive charges was detonated sequentially on improved and unimproved test areas to evaluate relative liquefaction resistance after RAP installation, monitoring excess pore pressures, settlements and accelerations. Also, four small exploratory trenches were dug to identify deformational features related to the blast tests and to characterize the fractures/conduits used by the liquefied sands during blast tests and in the 2012 earthquake. Samples of ejecta and in-situ sand were collected to characterize the soil deposits with geotechnical and/or petrographic laboratory tests. This combination of geological and geotechnical methods appears to be vital for a proper interpretation of the liquefaction process and for verifying the seismic origin of dykes (Obermeier, 1998). The paper describes the testing program and presents insights

from this multidisciplinary study.

2. Geology, geomorphology, and seismotectonic framework of the study area

2.1. Geological setting

The blast test site area is located in the south-eastern portion of the Quaternary alluvial plain which extends between the southern Alps and the northern Apennines. This plain is one of the deepest alluvial plain in Europe, though the exact depth of the seismic bedrock and the relevant seismic-wave properties are still a matter of debate among researchers (Molinari et al., 2015). The test site lies on the buried external portions of the Apennine chain, consisting of seismically active fault-fold structures (Toscani et al., 2009). The sedimentary units involved in the experiment accumulated during the late Pleistocene and Holocene periods, and show significant lateral variability in thickness (Minarelli et al., 2016). The latest Pleistocene unit is part of a depositional cycle typically referred to as Villa Verrucchio Subsynthem (AES7), whereas the Holocene sediments pertain to the Ravenna Subsynthem (AES8).

Several generations of fluvial channel deposits were fed from the south by the Apennine streams and from the west by the Po River (Fig. 1).

2.2. Seismic activity and effects

The area has a seismic history of low- to moderate-magnitude events. The most relevant past event is the VIII MCS (moment magnitude M_w 5.5) 1570 earthquake that struck the area of Ferrara, causing liquefaction phenomena, open fractures and changes in channel water flows (Caputo et al., 2016). In May 2012, a seismic sequence affected the area with two main shocks (Pondrelli et al., 2012). The first occurred on May 20th (M_w 6.1), with an epicenter at about 15 km to the south-west of the test site, followed by aftershocks up to M_w 5.1. The second main seismic event took place on May 29th (M_w 5.9), with an epicenter located at about 24 km to the south-west of the test site. The highest peak ground accelerations (PGA) recorded at nearby strong-motion stations located in the epicentral area turned out to be approximately 0.3 g and 0.9 g, for the horizontal and vertical components, respectively (Luzi et al., 2013). Both main shocks induced important secondary effects at the surface, such as widespread liquefaction, sand

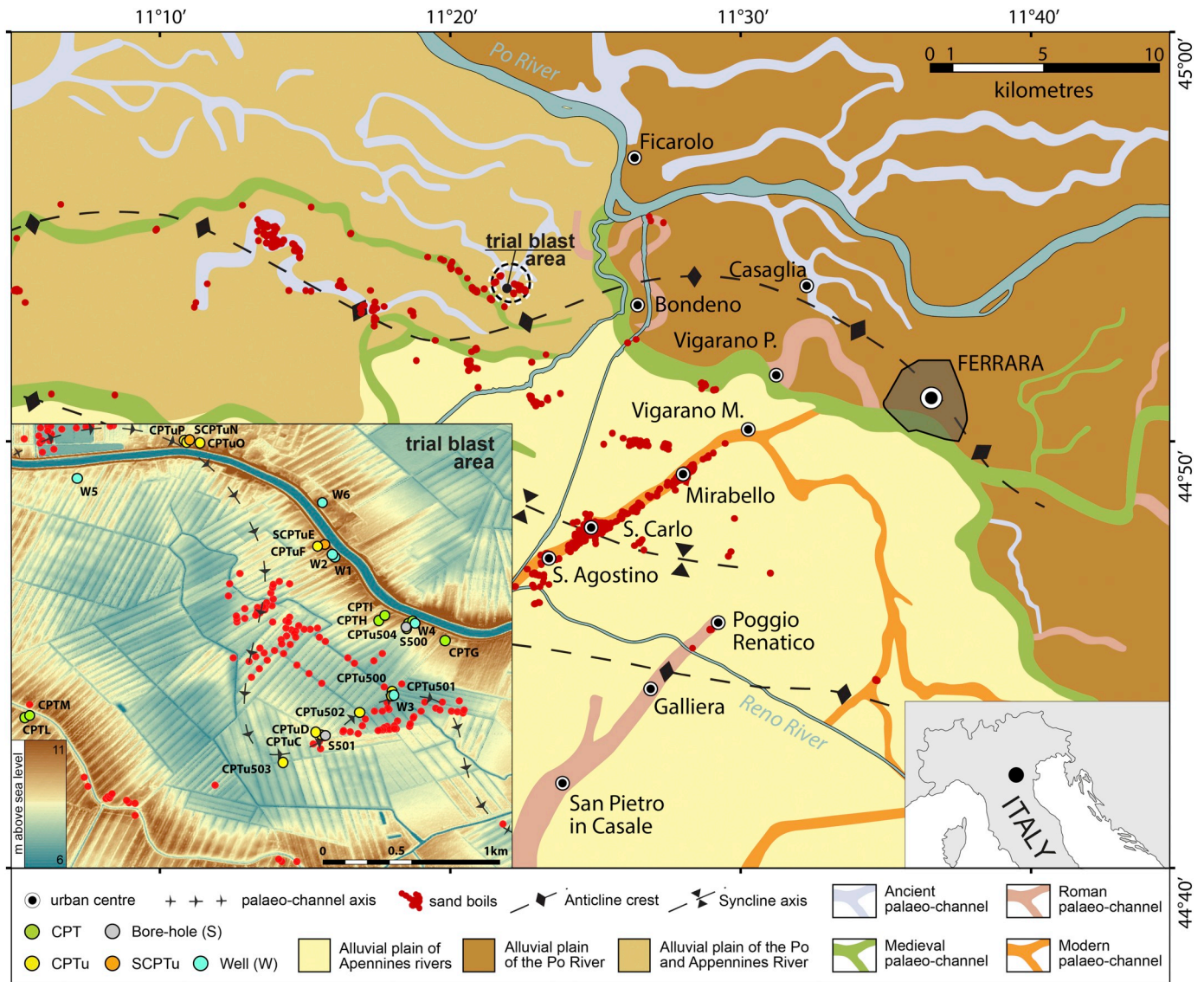


Fig. 1. Map of the paleochannel bodies (modified after Stefani et al., 2018), of the surface manifestations of liquefaction following the 2012 Emilia-Romagna earthquake (Emergeo Working Group, 2013) and of the location of the blast area. The traces of the main anticline crest and syncline axis of the buried tectonic belt are also depicted. The lower-left corner shows the geomorphological features from LIDAR map together with the available investigations and the 2012 sand boils.

boils (Fig. 1) and ground failures, together with lateral spreading and differential settlements. Sand boils and liquefaction manifestations occurred mainly along paleochannel deposits (Fig. 1).

2.3. Geomorphological framework

A strong link between the geographic distribution of the fluvial sand deposits and the location of liquefaction events was observed for the 2012 seismic crisis (e.g. Papathanassiou et al., 2015; Caputo et al., 2016) using satellite images and high-resolution LIDAR topographic models (Civico et al., 2015). The detected geomorphological features were also documented by the comprehensive database of subsurface investigations collected for the ongoing seismic microzonation (Fig. 1) and by other studies (Amoroso et al., 2020; Tonni et al., 2015).

The selected test site, which experienced the occurrence of a large number of sand boils (Fig. 1) during the 2012 seismic sequence (Emergeo Working Group, 2013), is located above a meander point bar structure. This meander morphology is partially confined by younger higher fluvial ridges bordering the test area in the south and the north (Fig. 1) and forming an interfluvial depression.

2.4. Stratigraphic organization

The fluvial sediments at the test site belong to three superimposed units, related to different depositional environments and chronological intervals (Figs. 1 and 4):

- (a) the lower unit consists of fluvial medium-grained sands and silty sands, deposited during the late glacial maximum (Pleistocene) into a braided river channel system (upper portion of AES7 unit). This unit is about 20 m-thick topped by a regional paleosol surface, overlain floodplain fine-grained sediments. At the test site, the top of this unit corresponds to the erosive base of a Holocene fluvial channel sand body;
- (b) the middle unit is formed by fluvial sandy silts, laterally grading into argillaceous sediments. This unit is approximately 9 m-thick (AES8 unit, Holocene). The interpretation of satellite images and topographic data, coupled with information obtained from subsurface logs, suggests that the sand accumulated into a meandering channel of the Po River. At the test site, this unit is buried at a shallow depth. The liquefaction induced by the blast test largely took place within this unit;
- (c) the upper unit comprises fluvial clays and silts (3 m-thick) forming the uppermost part of the AES8 unit, deposited during the final infilling of the fluvial channel, probably recording influxes from Apennine-derived rivers.

3. Description of the field activities

The blast tests activities were conducted over a period of 1 year (November 2017–October 2018), as listed in Table 1.

From November 2017 to January 2018, preliminary investigations

Table 1

Activities associated with blast tests at Bondeno site.

Phase	Activity	Period
I	Preliminary investigations for site selection	November 2017–January 2018
II	Geotechnical and geophysical tests for characterization of the test site	February–March 2018
III	RAP column installation	March–April 2018
IV	Geotechnical and geophysical tests 1 month after RAP installation	April–May 2018
V	Installation of blast holes, profilometers, accelerometers, pore pressure transducers	May 2018
VI	Blast tests	4 June 2018
VII	Geotechnical and geophysical tests soon after blast tests	June 2018
VIII	Geotechnical and geophysical tests 1 month and a half to 2 months after blast tests	July–August 2018
IX	Geological, geotechnical and geophysical tests 3 to 4 months after blast tests	September–October 2018

were aimed at identifying the most suitable test site. This choice was guided by the need to select a shallow liquefiable layer of silty sands, also taking into account the previously mentioned geomorphological considerations and 2012 liquefaction evidences. Furthermore, the site was located at a distance from buildings and human activities of this area in order to minimize the effect of vibrations generated by the detonation.

3.1. Pre-blast activities

3.1.1. Pre-RAP investigations

From February to March 2018 an intensive geotechnical and geophysical campaign was carried out in order to achieve a detailed characterization of the upper 20 m of the subsoil, also useful for the design of the RAP columns and the blast tests. These surveys allowed identifying a relatively homogeneous area (60 m × 40 m), where two blast panels – one for testing the natural soil (Natural Panel, NP) and one for the improved soil (Improved Panel, IP) – were eventually placed (Fig. 2a and b). Later investigations were all concentrated in these two relatively small circular areas spaced 20 m apart, each having a diameter of 10 m. The geotechnical investigations, pushed to approximately 15–20 m in depth, consisted of: (i) two boreholes, one in the IP and one in the NP, along with standard penetration testing (SPT) and disturbed soil sampling for grain size distribution analyses, determination of Atterberg limits, petrographic analyses and radiocarbon dating; (ii) two piezocone (CPTU) tests, one in the IP and one in the NP; (iii) one seismic dilatometer (SDMT) test in the IP. The geophysical surveys consisted of: (i) five electrical resistivity tomography (ERT) alignments, spaced at 2–5 m and 63 m long (64 electrodes for each line), crossing the IP and the NP; (ii) one active P-wave and S-wave tomography, 71 m long, performed using firstly 72 vertical geophones and secondly 72 horizontal geophones along the same line; and (iii) one passive 2D-rectangular array (24 m × 21 m) using 72 P-wave geophones spaced at 3 m, and centered in the IP.

Grain size analyses were carried out using a Mastersizer 3000 particle size. Compositional analyses under transmitted light microscopy were performed on the 0.125–0.250 mm fraction, according to the Gazzi-Dickinson method, designed to minimize the dependence of the analysis on the grain-size (Fontana et al., 2015).

Prior to RAP installation, a 0.5 m-thick, geosynthetic-reinforced, gravel platform was set up to allow the access of the RAP installation equipment machinery. Moreover, an additional CPTU was performed to check the IP homogeneity, and a SDMT was also performed within the NP.

3.1.2. RAP installation

Between the end of March and the beginning of April 2018, a 4 × 4 quadrangular grid (2 m center-to-center spacing) of RAP columns, each 9.5 m long, was built (Fig. 2). The final diameter of each pier was 0.5 m with an associated area replacement ratio, defined as the ratio of the pier area to the tributary soil area surrounding the pier, equal to 5%. Because of construction issues, the last column of the third line was

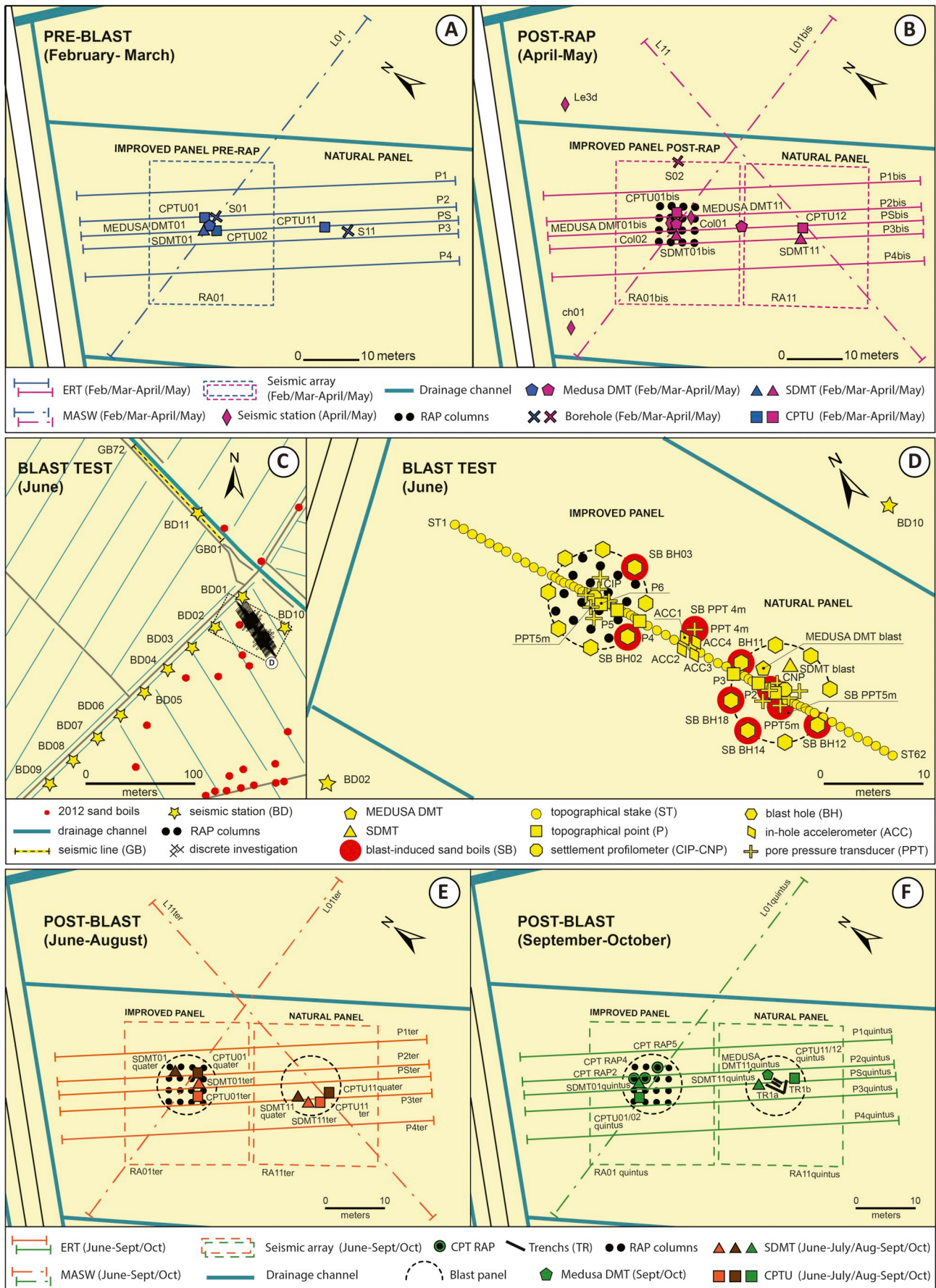


Fig. 2. Map of the investigations at the test site carried out pre-blast in February–March 2018 (a), post-RAP in April–May 2018 (b), during blast at small (c) and large (d) scale, post-blast in June–July–August 2018 (e) and in September–October 2018 (f).

limited to only 5.5 m depth. For quality control of the ground improvement work, ten RAPs were subjected to aggregate flow rate tests and crowd stabilization tests in order to evaluate the pier gravel volume and to measure the column stiffness, respectively. These tests revealed a reduced effectiveness of the construction procedure for the upper-left piers.

The RAP elements were constructed using a displacement technique with an excavator mounted mobile ram base machine fitted with a high frequency (30–40 Hz) vertically oscillating hammer as illustrated in Fig. 3.

The base machine drives a 300 mm outside diameter open-ended pipe mandrel fitted with a unique specially-designed 360 mm diameter tamper foot into the ground. Proprietary internal restrictor elements prevent soil from entering the mandrel during driving and serve as an internal compaction surface during tamping. After driving to the designed depth, the hollow mandrel serves as a conduit for aggregate placement. Placed inside, the aggregate flows to the bottom of the mandrel. The tamper foot and mandrel are then raised approximately 0.9 m and then driven back down 0.6 m, forming a 0.3 m-thick compacted lift. Compaction is achieved through static down force and dynamic vertical ramming from the hammer combined with the confinement of the tamper's restrictor elements. The process densifies aggregate vertically and the beveled tamper foot forces aggregate laterally into cavity sidewalls. Crushed gravel (typically graded at 10–40 mm in particle size) is fed through the mandrel from a top mounted hopper and compacted in the displaced cavities to create approximately a 0.5 m-diameter, dense, stiff, aggregate pier element. The construction methodology has been described in detail by Saftner et al. (2018).

3.1.3. Post-RAP investigations

At the end of April 2018 supplementary geotechnical tests were carried out in the middle of four piers (Fig. 2b) and pushed to a maximum depth of 15 m, in order to evaluate the RAP effect on soil response 1 month after construction. DMT soundings were performed using a new device, the Medusa DMT, that is a combination of the flat dilatometer with hydraulic automation and a measuring system for autonomously performing DMT tests (Marchetti et al., 2019).

At the beginning of May 2018, the temporary gravel platform was removed to allow additional geophysical surveys with the same configuration as the original investigation (Fig. 2b): (i) five ERT

alignments; (ii) two active P-wave and S-wave tomographies, one in the IP and one in the NP; (iii) two passive 2D-rectangular arrays, one centered in the IP and one centered in the NP; and (iv) four surface seismic stations, equipped with three-components Lennartz-5 s velocimeter, two in the treated area and two in the natural soil.

3.2. Blast activities

In May 2018, blast holes, profilometers, accelerometers, pore pressure transducers, seismic DMT and Medusa DMT equipment were installed in the ground. Topographical reference points, seismic stations and geophones were placed on the surface in preparation for the blast tests that took place on June 4th, 2018 (Fig. 2c and d). Locations of the instrumentation relative to the blast holes for each panel are shown in Fig. 2d.

Eight blast holes (BH), 7 m deep and equally distributed along a 5 m-radius ring, were drilled in each panel. Charges were located in each BH at 3.5 m (0.5 kg) and 6.5 m (2.0 kg) within the potentially liquefiable layer. This soil layer was detected between 3 and 8 m depth according to a preliminary assessment of liquefaction susceptibility, that considered a design earthquake for a 475 years return period ($M_w = 6.14$ and $PGA = 0.22$ g, Amoroso et al., 2019).

At the center of each panel, a profilometer (CNP for the natural panel and CIP for the improved panel) was anchored at 15 m depth to record the settlement vs. depth profile. In fact, previous experiences worldwide (e.g. Amoroso et al., 2017; Gianella and Stuedlein, 2017; Finno et al., 2016) provided evidence of a bowl shaped displacement surface following blasting. Furthermore, from the previous blast experiment carried out in a site of the Po River valley, it was observed that settlements in the circular blasting area were similar to liquefaction-induced vertical displacements predicted for a M_w 7.5 earthquake in the same depth interval (Amoroso et al., 2017).

To estimate blast-induced shear strains and shear stresses, four in-hole 200 g triaxial microelectromechanical (MEMS) accelerometers (ACC) were located at approximately midway between the two panels (i.e. about 10 m from CNP and CIP), using a 1 m-squared configuration between 3.5 and 4.5 m deep and recorded at a sampling rate of 1000 Hz. Pore pressure transducers (PPT) were installed from 4 to 9 m at each meter of depth, within the liquefiable layer (1 or 2 m distance from the center of each panel) to measure the generation and subsequent dissipation of the excess pore pressures induced by the blasts in

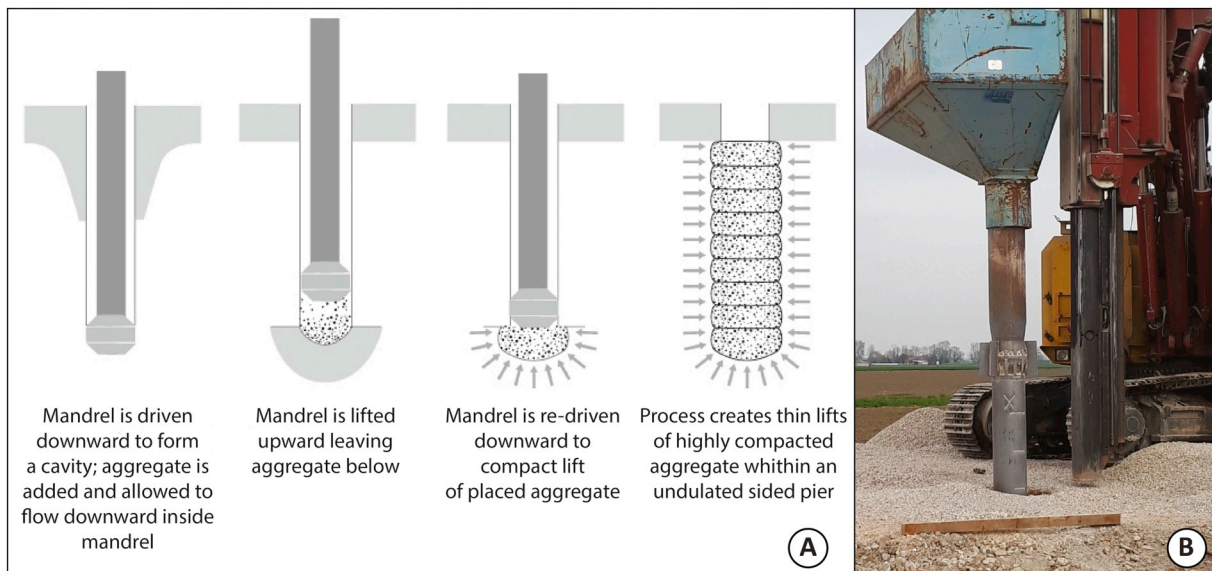


Fig. 3. (a) RAP column installation scheme with vibratory hammer and hopper/mandrel for gravel installation (Wissmann et al., 2015); (b) RAP installation at Bondeno test site.

the silty sand deposits of both panels, at a sampling rate of 100 Hz. An additional PPT was set up at an average depth of 4 m in the middle of the accelerometer array to study the non-linear soil response induced by the blast-liquefaction, coupling the shear strains with the excess pore pressures. A SDMT and a Medusa DMT were finally installed at 6.1 m deep in the natural panel to monitor the variation of shear wave velocity with excess pore pressure following the blasts.

Six survey rods (P) were located within the NP and the IP and an alignment of 62 survey stakes (ST) crossing both panels was set up to record the vertical ground surface settlements over time after the blasts and to integrate with the profilometer data, Terrestrial Laser Scanning (TLS), and Structure from Motion (SfM) aerial photogrammetry. A line of 72 P-wave geophones (GB, 4.5 Hz) was installed at an average distance of 100 m from the blast area, while 11 surface seismic stations (BD), each of them composed of a velocimeter (Lennartz-5 s) and an accelerometer (Episensor-1 s), were located along a Y-shaped configuration, having the closest and the farthest stations at 25 and 250 m, respectively (Fig. 2c), to record the particle motion with distance and to verify the level of vibration generated by the detonation.

Explosives were detonated on June 4th, with a microdelay of 1 s between subsequent charges and starting the detonation from the bottom (6.5 m deep) to the upper level (3.5 m deep). The blasts of the two panels were designed separately (i.e. blast #1 for the NP and blast #2 for the IP) to limit effects of superposition and consequently to study the effect of the blast-induced liquefaction on the IP and the NP separately.

Surface movements induced by underground explosions and liquefaction effects were observed by means of TLS and SfM surveys performed before and after each blast test providing and comparing multi-temporal Digital Terrain Models (DTMs). Unmanned Aerial Systems (UAS) equipped with DJI FC6310 and DJI FC350 cameras and a Teledyne Polaris scanner were used. The results from TLS dense point clouds, characterized by a mean 5 mm sampling step, provide a complete description of subsidence rates in the area following liquefaction and pore pressure dissipation.

3.3. Post-blast activities

Three post-blast investigations were performed in June, July–August and September–October 2018 (Fig. 2e and f), with the aim of comparing the variation with time of the geotechnical and geophysical parameters before and after the blast tests in both panels.

Two piezocone and two seismic dilatometer tests were carried out up to 15 m deep, in the IP and the NP soon after the blast tests. Moreover, in June 2018 ERT surveys and active and passive geophysical surveys were performed using the same configuration of the previous investigations shown in Fig. 2e.

One month and a half to two months after the blast tests, an additional in-situ testing campaign was repeated: two CPTUs and two SDMTs were performed, up to 15 m deep, between piers and within the untreated area, as shown in Fig. 2e.

Finally, 3–4 months after blasting, the last geotechnical and geophysical tests were carried out, as reported in Fig. 2f. As for the previous investigations, CPTUs, SDMTs and Medusa DMTs were performed in the IP and the NP, pushing tests to a maximum depth of 15 m. Moreover, three mechanical cone penetration tests were performed at the center of RAP piers (CPT RAP) to a depth of approximately 11 m. In September–October 2018 ERT, active and passive geophysical surveys were repeated again using the same configuration of the previous investigations.

At the conclusion of the experimental activities, four small exploratory trenches were dug across the liquefaction-induced sand boils within the natural panel (Fig. 2f). The excavations were performed to better understand the blast-induced liquefaction mechanism but also to identify and characterize the fractures/conduits used by the liquefied sands in the 2012 earthquake (Amoroso et al., 2017) and possibly during older events (De Martini et al., 2012; Caputo et al., 2016). Moreover, sand samples were collected from the fractures as well as from the surface (sand boils) in order to study the variability in grain size potentially related to the liquefaction process and to the liquefied sand paths (Fontana et al., 2019).

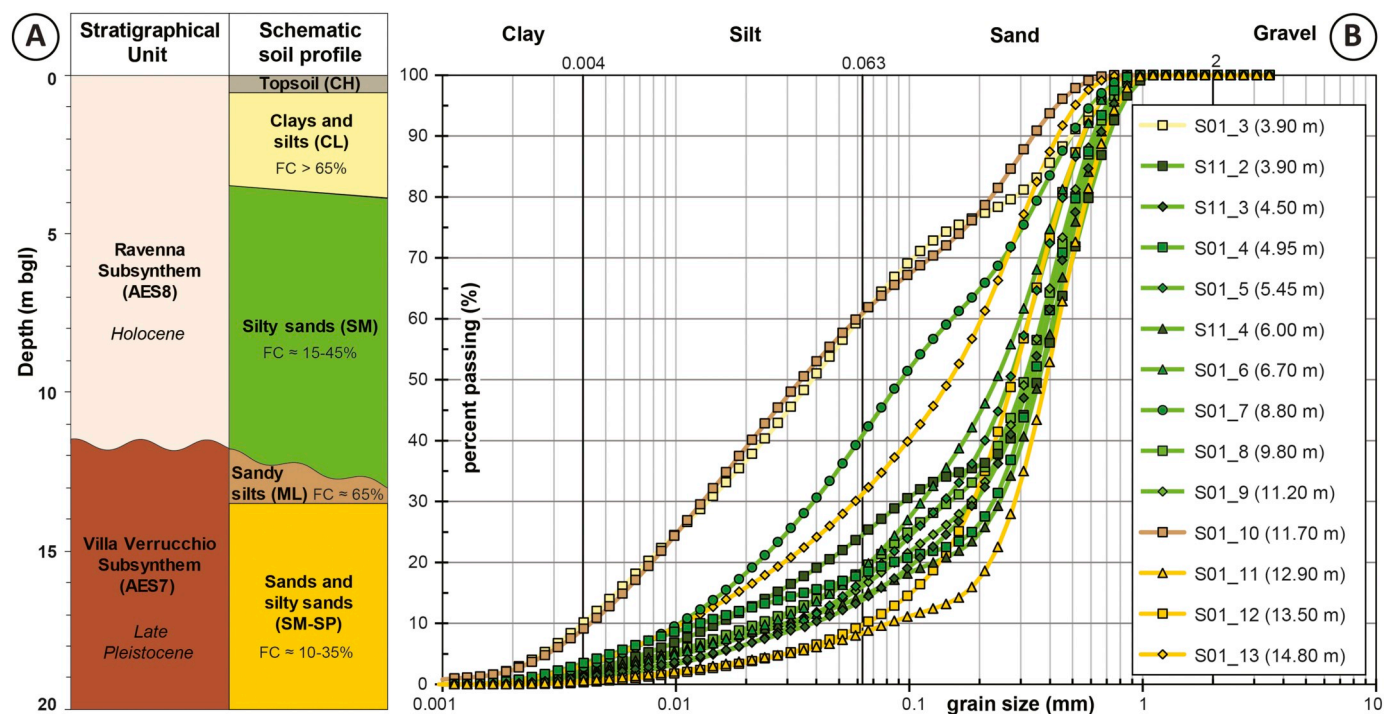


Fig. 4. Average subsoil profile at the test site and stratigraphic units (a) and grain size analyses (b).

4. Main geotechnical features from the pre-blast investigations

The interpretation of all the geotechnical and geophysical investigations performed in both panels (IP, NP) prior to improvement was used to define a representative stratigraphic model of the natural subsoil (Fig. 4a). The identified soil units are listed below and classified in terms of the Unified Soil Classification System (USCS), according to ASTM D2487-11 (2011):

- (i) top soil (CH) from the ground surface to 0.8 m;
- (ii) clays and silts (CL) from 0.8 to 3.4 m;
- (iii) silty sands (SM) from 3.4 to 12.6 m (paleochannel of the Po River);
- (iv) sandy silts (ML) from 12.6 to 13.4 m (well-drained interfluvial deposits);
- (v) sands and silty sands (SM-SP) from 13.4 to 15.6 m (glacial braided Po River deposits).

The silty sands (SM) and sandy silts (ML) have laterally a variable thickness due to their channel-filling nature. In this respect, the ML layer can vary in depth between 11.70 and 13.40 m, and have a minimum thickness of approximately 0.5 m.

Fig. 4b shows the results of the grain size analyses performed on the disturbed samples from S01 and S11 boreholes. The analyzed samples range from silty sands to silts with a variable amount of sand and clay. The majority of samples fits in a relatively narrow range, predominantly made up of fine sands; the content of silt is on average < 25% and clay is < 5%. A higher percentage of fine sediments can be found in the shallowest sands (3.9 m depth) or in thin lenses detected at 8.8, 11.7 and 14.8 m depth. In particular, Fig. 4 shows that the SM layer has a fine content $FC \approx 15\text{--}45\%$, while $FC \approx 65\%$ for the ML layer and $FC \approx 10\text{--}35\%$ for the SM-SP layer.

Sands from cores S01 and S11 have a quartz-feldspar rich composition and are made up of quartz, feldspars and subordinate lithic fragments. Siliciclastic lithics include low-grade metamorphic rocks, shales and spillite and carbonate lithic. Crystals of muscovite, chlorite

and biotite are also present as well as heavy minerals. The composition of the sands show a clear affinity with sands from the Po River.

With reference to the defined stratigraphic model, Fig. 5 shows the soil response prior to RAP installation in terms of corrected cone resistance (q_t) from CPTU test, horizontal stress index (K_D) and shear wave velocity (V_S) from the SDMT test. The variation of q_t and K_D profiles with depth looks related to the geologic depositional environment. Below the fine-grained units detected in the upper 3.4 m, the paleochannel of the Po River (from 3.4 to 12 m) is characterized by different q_t and K_D values when compared with glacial braided Po River deposits (below 13.4 m). In contrast, the V_S increases consistently with the effective vertical stress.

Fig. 5 also provides interpretations of CPTU measurements in terms of the soil behavior type index (I_{cn}), fines content (FC) according to Robertson and Wride (1998), and relative density (D_R) computed with the correlation proposed by Jamiolkowski et al. (2003). The computed FC values appear to be generally underestimated in comparison with those obtained from laboratory tests (blue dots in Fig. 5). However, at the test site the dataset is currently too small to develop a site-specific correlation that would take into account the uncertainties related to FC - I_{cn} relationship (e.g. plasticity and mineralogy).

5. Main outcomes from the experimental activities

5.1. Post-RAP investigations

The site investigation performed 1 month after RAP column installation was helpful to understand the effectiveness of the ground improvement technique. Fig. 5 provides a comparison between field soil responses before and after treatment, in terms of both CPTU and SDMT profiles. A decrease of soil properties in the upper crust, partly due to the construction of the platform, but also to the low confinement induced by RAP installation and the seasonal variations in water content caused by fluctuation of the GWT from 1.5 m (February 2018) to 0.8 m (April 2018), is observed. Conversely, the layer between 3.4 and

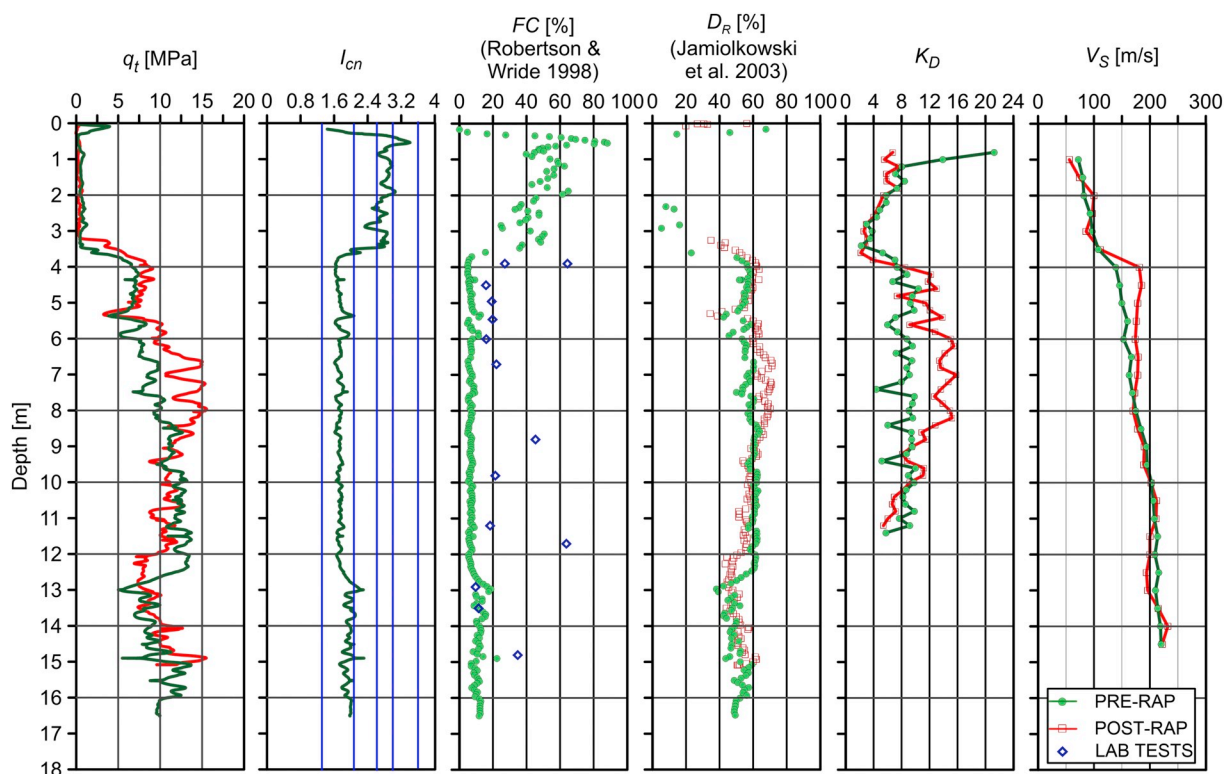


Fig. 5. CPTU and SDMT profiles pre/post RAP installation.

9.5 m shows an increase in resistance and stiffness due to the installation of the piers. Unlike clean sands studied in New Zealand (e.g. Wissmann et al., 2015; Vautherin et al., 2017), in this case no improvement was detected in the silty sands below the toe of piers (Fig. 5). Looking in detail at the in-situ test data between 3.5 and 5.5 m depths, q_t and K_D increase on average from 7 to 8 MPa, and from 7–9 to 12, respectively. This trend is further confirmed in the underlying layer, between 5.5 and 9.5 m, where the natural soil is characterized by $q_t \approx 8$ –10 MPa and $K_D \approx 7$ –9, and the treated soil assumes values of $q_t \approx 10$ –14 kPa and $K_D \approx 13$ –15. Moreover, from 3.5 to 5.5 m in depth, the CPTU-based estimates of D_R shows a minor increase after pier installation, whereas a more significant increase is observed at 5.5–9.5 m (i.e. from approximately 60 to 70%). In contrast, V_s measurements show a limited improvement between 4 and 7 m depth, from 140–165 to 175–185 m/s, and remain constant below 7 m (Fig. 5). This tendency may be related to the decrease in vertical effective stress with some disturbance to the soil structure (e.g. Mitchell and Solyman, 1984), for RAP installation.

5.2. Blast test effects

Fig. 6a and b show the results of the aerial SfM survey after both blasts. It can be easily observed that liquefaction was induced in the NP, as clearly indicated by the widespread sand boil evidence in this location (see also Fig. 2d). In contrast, only minor liquefaction traces are observed within the IP, mainly near the edge of the blast ring. These limited sand boils are, however, outside the limits of the RAP group and likely developed in unimproved soils in this area.

Fig. 6c documents the sand boils induced by the blast in the NP after blast #1. Grain size distribution analyses on soil samples collected from the sand boils (green curves in Fig. 6d) detected medium-grained sands with a fines content varying between 6 and 28%. Compared to grain size characteristics of the source beds (i.e. SM layer, red curves in Fig. 6d), a selective loss of fines can be appreciated in the ejected sediments forming the sand boils, thus indicating that the liquefaction process appears to preferentially select the grain diameters, as previously found by Fontana et al. (2019), Maurer et al. (2019) and Cubrinovski et al. (2018).

Pore pressures measured by the PPT were used to compute excess pore pressure ratios ($R_u = \Delta u / \sigma'_{v0}$) in the NP and the IP, where Δu is the measured excess pore pressure and σ'_{v0} is the initial vertical effective stress prior to the blasts. Soil unit weights were interpreted from the SDMT tests. In the NP, R_u values reached 1.0, indicating liquefaction, from a depth of 4 to 9 m. Plots of R_u versus time after blasts are presented in Fig. 7 for transducers at a depth of 5 m in the IP and the NP. In the NP, the blast sequence produced R_u values near 1.0 which persisted for 15 to 30 s (see the zoom in Fig. 7) and then dissipated to near static levels in about 4 min. In the IP, peak R_u values were somewhat lower ($R_u = 0.75$) than in the NP, but dissipated at a similar rate.

Settlement profilometers indicated that liquefaction, and subsequent reconsolidation, occurred within a zone from about 3 to 11 m below the ground surface which is generally consistent with the expected zone of liquefiable sediments. In the NP, volumetric strains were consistent with what would be predicted by Zhang et al. (2002) if a M_w 7.5 earthquake had produced liquefaction from 3 to 11 m with a factor of safety of about 0.9. Volumetric strains in the same depth interval for

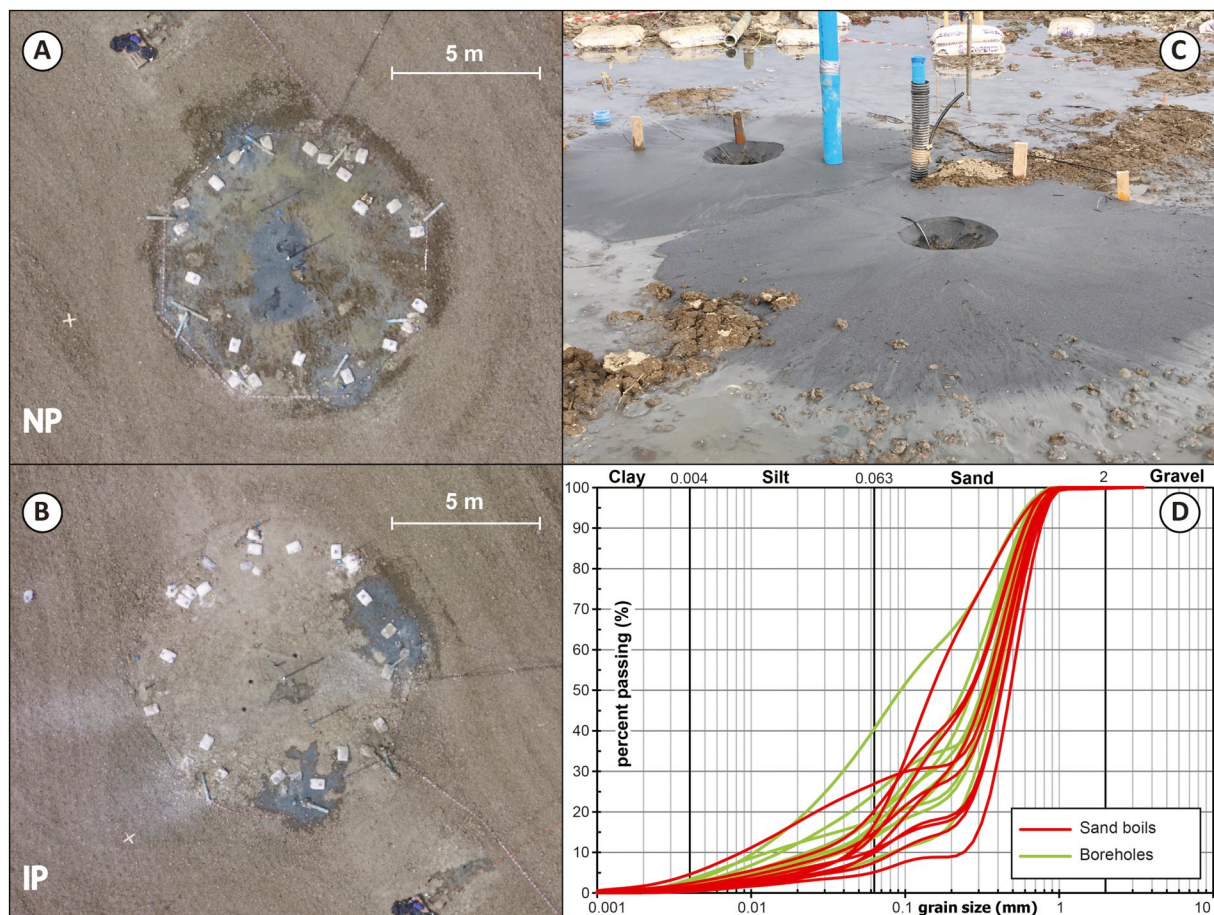


Fig. 6. SfM point cloud of surveyed area showing liquefaction-induced sand boils after blast #1 in the NP (a) and blast #2 in the IP (b). Detail of the sand boils in the NP (c); grain size distributions of the sand boils (in red) compared with sands from the boreholes (in green) (d). (For interpretation of the references to colour in this figure legend, the reader is referred to the web version of this article.)

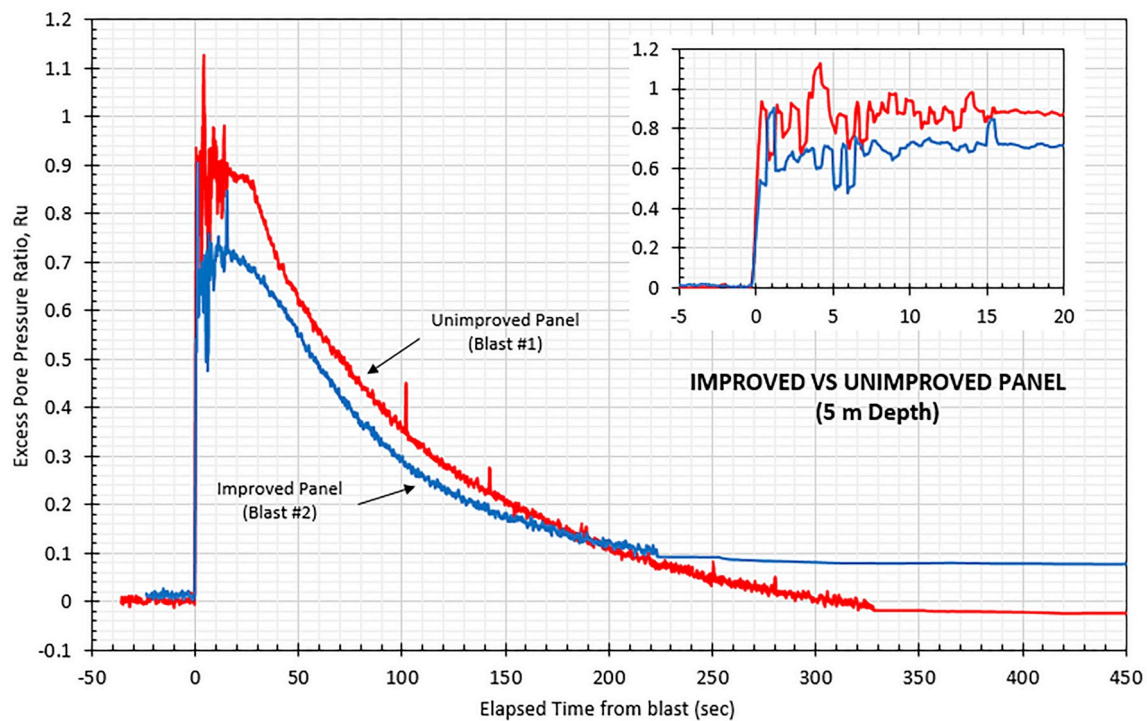


Fig. 7. Comparison of measured excess pore pressure vs. time curves for the IP and the NP at a depth of 5 m below the ground surface. For both panels the PPTs recorded at a sampling rate of 100 Hz and the R_u values were smoothed using a 100 point running average. This was done so that the residual excess pore pressure would not be obscured by the transient pressure spikes.

the IP were about 20% of those measured for the NP, despite excess pore water pressure values that resulted in R_u values of 0.7–0.9.

Fig. 8 shows colour settlement contour maps obtained by comparing the TLS-based multi-temporal models with the terrain morphology maps. In the NP, after blast #1 there is clear subsidence of the area within the explosive charges, with a widely distributed settlement of about 6–8 cm. In contrast, after blast #2 only a few small sectors of the IP experienced settlement with an average of 2 cm (locally maximum 4–5 cm). For both blast tests, settlements were mainly delimited within about 10 m from the centers of the blast areas.

All topographical surveys indicate that settlements within the NP were on average between 7 and 10 cm, after both blasts. In contrast, settlements within the IP were between 2 and 5 cm. Liquefaction induced settlements in the NP would likely be excessive for many structures, whereas the reduced settlements in the IP would likely be tolerable. The mechanisms responsible for the reduced settlement in the panel treated with RAP columns may be related to soil densification and increased lateral stress, but soil-pier interactions may also play a role. Due to the whole test setup the bearing capacity was not evaluated, even though it is another important issue within liquefaction evaluation criteria.

Fig. 9 shows the SDMT results recorded in the NP during both blasts. Soon after the blast #1, the SDMT data show a shear wave velocity decrease to about 30% of its pre-blast value ($V_s \approx 49$ m/s versus $V_s \approx 152$ m/s), while it took a few minutes to recover to approximately its initial value. For blast #2, since the SDMT modulus was still installed in the NP, a smaller decrease of shear wave velocity is observed, equal to approximately 5% of its pre-blast value ($V_s \approx 141$ m/s in place of $V_s \approx 149$ m/s), associated with a much faster recovery to its initial value. These results are consistent with other previous experiences (e.g. Rollins et al., 2004; Mahvelati et al., 2016). Blast-induced liquefaction reduces indeed the vertical effective stress and alters the soil fabric, thus causing initial losses in soil stiffness (Mitchell and Solymar, 1984). However, the dissipation of the excess pore pressure allows the soil to reconsolidate into a denser and more stable configuration (Narin van

Court and Mitchell, 1994) characterized by a higher soil stiffness, as confirmed also at the Bondeno trial site by R_u and V_s data (Figs. 7 and 9).

All the seismic instruments installed prior to the blast tests (Fig. 2c and d) recorded the signals produced by both detonations. Particularly, Fig. 10 shows some examples of time-series recorded by the in-hole accelerometers. The detonations performed at 6.5 m depth produced very energetic signals that are clearly recognizable in both the time and frequency domains (Fig. 10b). Instead, the signals recorded at 3.5 m depth have generally lower amplitude, compared to the deeper ones, and, in some cases, they are difficult to detect in the recorded time-series. The seismic data produced during each blast are characterized by a very impulsive signal of short duration (about 0.02 s) and high amplitude followed by a coda having a lower amplitude and a frequency content below 25 Hz (Fig. 10b). For each detonation, the duration of the entire recorded signal does not exceed 0.4 s (Fig. 10b and d). The maximum peak acceleration recorded by the in-hole sensors was of about 45 g (ACC2-Y in Fig. 10c) and 52 g during blast #1 (NP) and blast #2 (IP), respectively. In both cases, the maximum acceleration was recorded by the Y-component of ACC2 sensor (Fig. 10a and d). From the spectrogram (Fig. 10b), the spectral content of the signals associated to explosions reach the maximum resolvable frequency (Nyquist frequency at 500 Hz) with the adopted sampling rate. Nevertheless, for each shot the maximum of signal was observed during the first impulse (Fig. 10c) with a duration of about 0.003 s, corresponding to frequency of about 300 Hz, a value lower than the Nyquist frequency.

The seismic stations and the geophones permitted an estimate of the peak ground acceleration (PGA) and peak ground velocity (PGV) values generated by both the blasts at distances between 20 and 250 m from the centers of the two panels. For blast #1, the maximum horizontal and vertical PGA were equal to 1.2 g and 1.3 g, while for blast #2 the values were 0.8 g and 3.6 g, respectively. In both cases, the blast-induced ground motion attenuated rapidly with distance and reached values smaller than 0.01 g at about 180 m distance. The PGV values

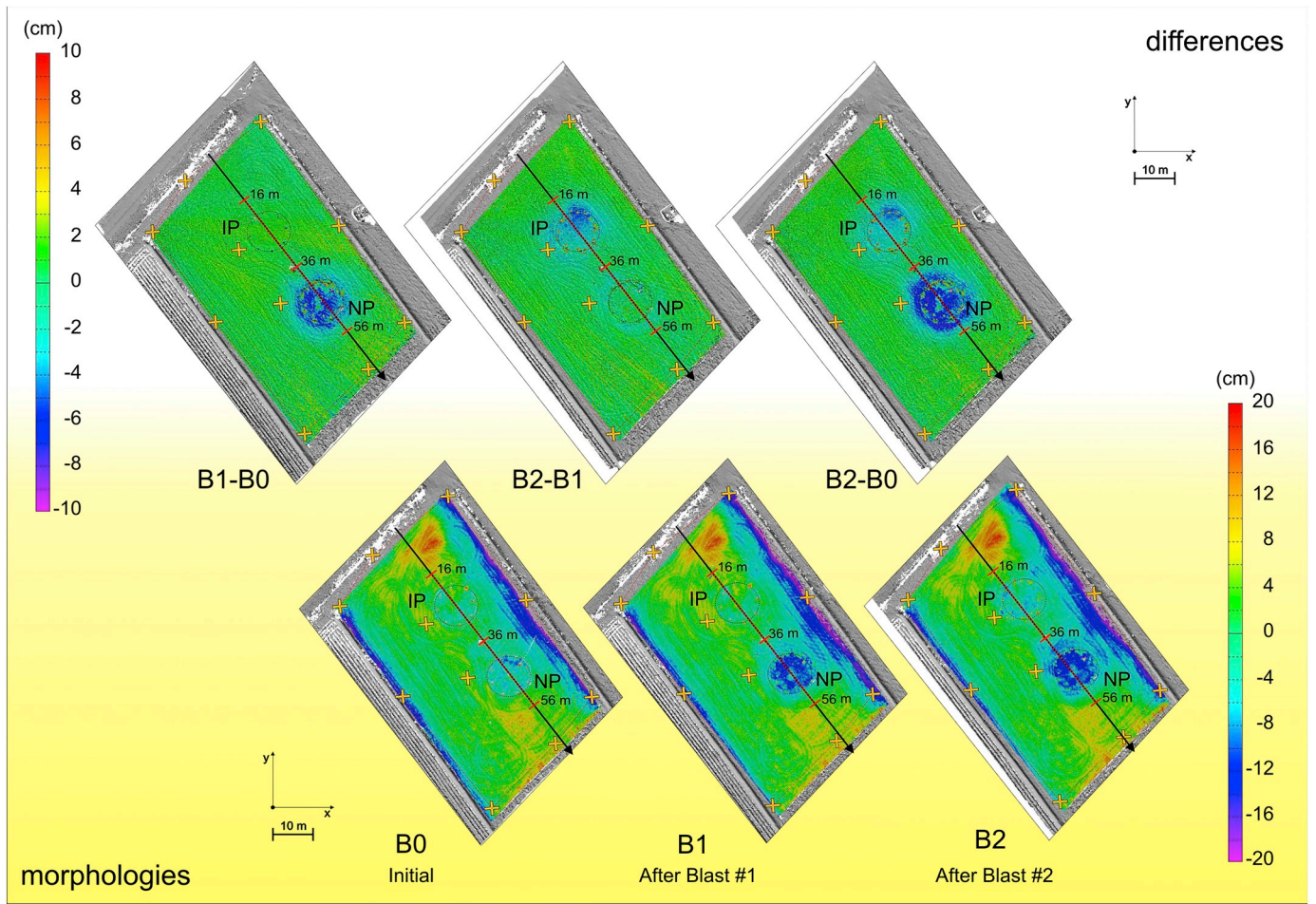


Fig. 8. Difference maps between TLS-based point clouds (upper panels), where BN-BM means N-th point cloud compared with respect to the M-th one, and morphological maps (lower panels).

provide an exponentially decreasing trend with distance, consistent with other field test evidences (e.g. Gianella and Stuedlein, 2017; Amoroso et al., 2017), recording ranges from 0.14 to 0.0007 m/s at 20 and 250 m distance from the blast centers, respectively.

5.3. Post-blast investigations and comparison to all previous data

Fig. 11 shows the comparisons between the average profiles of q_t , K_D

and V_s acquired in the pre- and post-blast investigation campaigns, for both panels. Error bars are displayed in order to take into account the variability of measurements within the different soil units.

With reference to the IP after blasting, the comparison of the piezocone results reveals a general slight increase of the corrected cone resistance in the silty sands (SM), although the ranges reported in Fig. 11b do not appear to differ significantly. Negligible changes in the q_t profiles can be appreciated within the lower sands/silty sands.

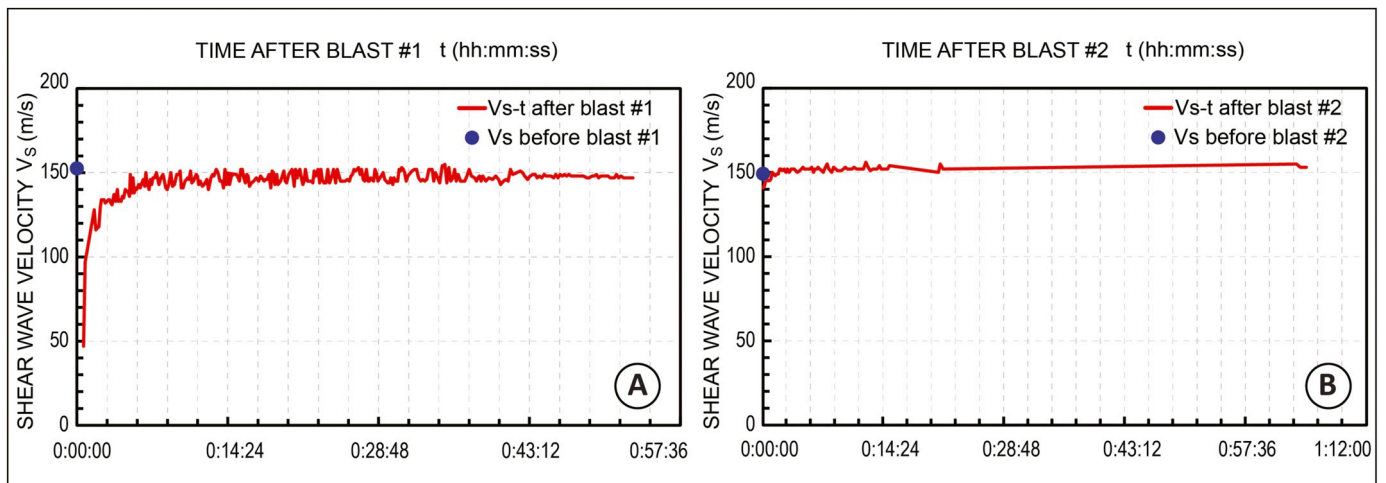


Fig. 9. Shear wave velocity data from seismic dilatometer during blasting: (a) blast #1; (b) blast #2.

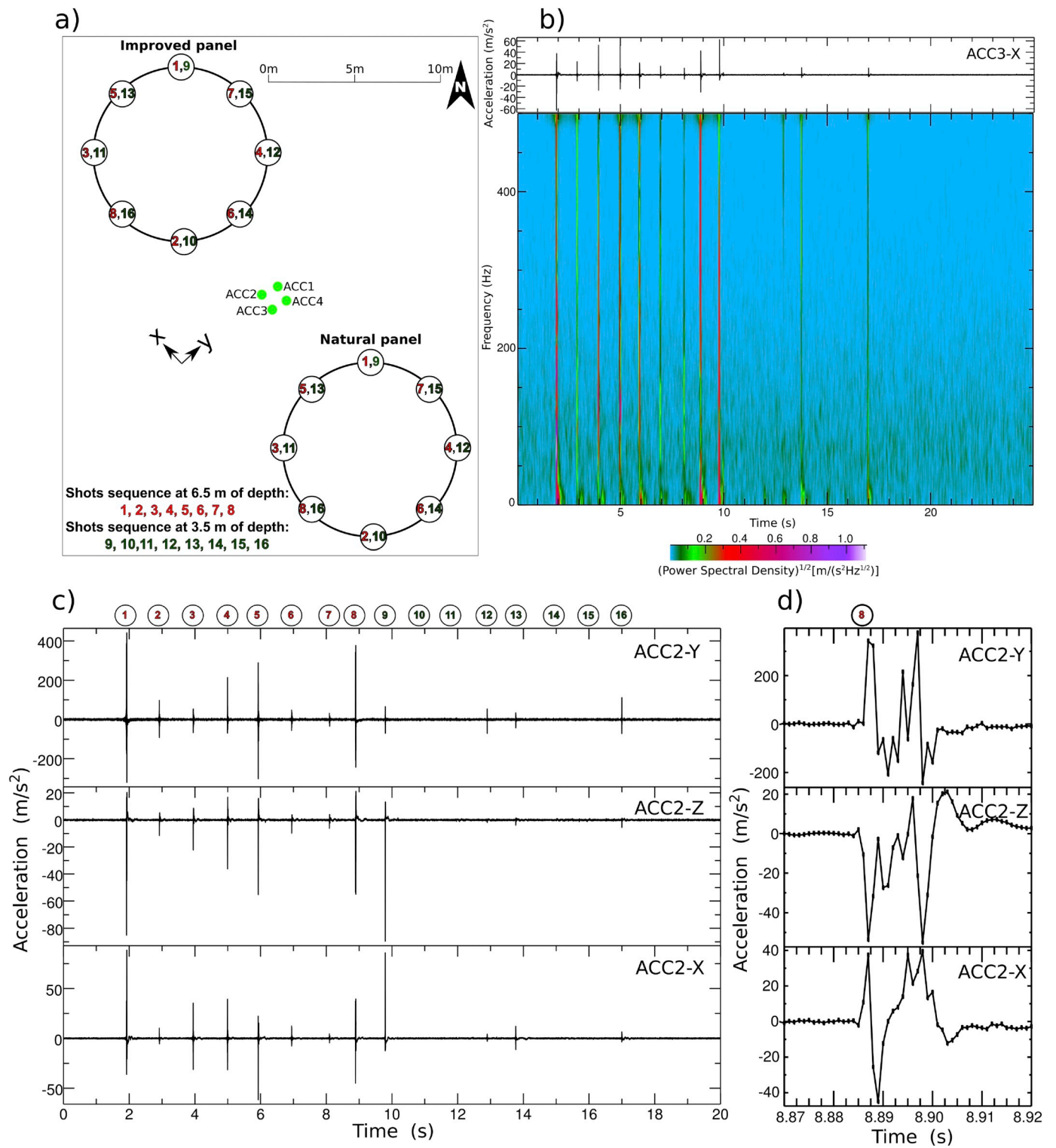


Fig. 10. Schematic diagram illustrating the locations (and the sequences) of charges detonated in the NP and the IP with respect to the positions of the four installed accelerometers (ACC1, ACC2, ACC3, ACC4) (a); seismic traces and related spectrogram recorded during blast #1 by the X-component of ACC3 in-hole accelerometer (b); time histories of accelerations recorded during blast #1 by the three different components of ACC2 accelerometer (c); zoom of signals recorded during blast #1 by the different components of ACC2 during the shot number 8. The circles on the top of Fig. 10c and d show the number of explosions associated with the recorded signals (d).

Similarly, the cone resistance profiles in the liquefied layer (3.4–9.5 m) of the NP (Fig. 11a) slightly increase with time (from June to July–August to September–October), whilst the underlying layers do not show any significant change, probably as a consequence of the charge locations. It is worth observing that the horizontal spatial variability of

the subsoil complicates at time the direct comparison of the different CPTU soundings.

Based on the DMT results, a few days after blasting, the horizontal stress index turned out to maintain approximately its average value within the liquefiable layer of the IP (Fig. 11b), confirming the

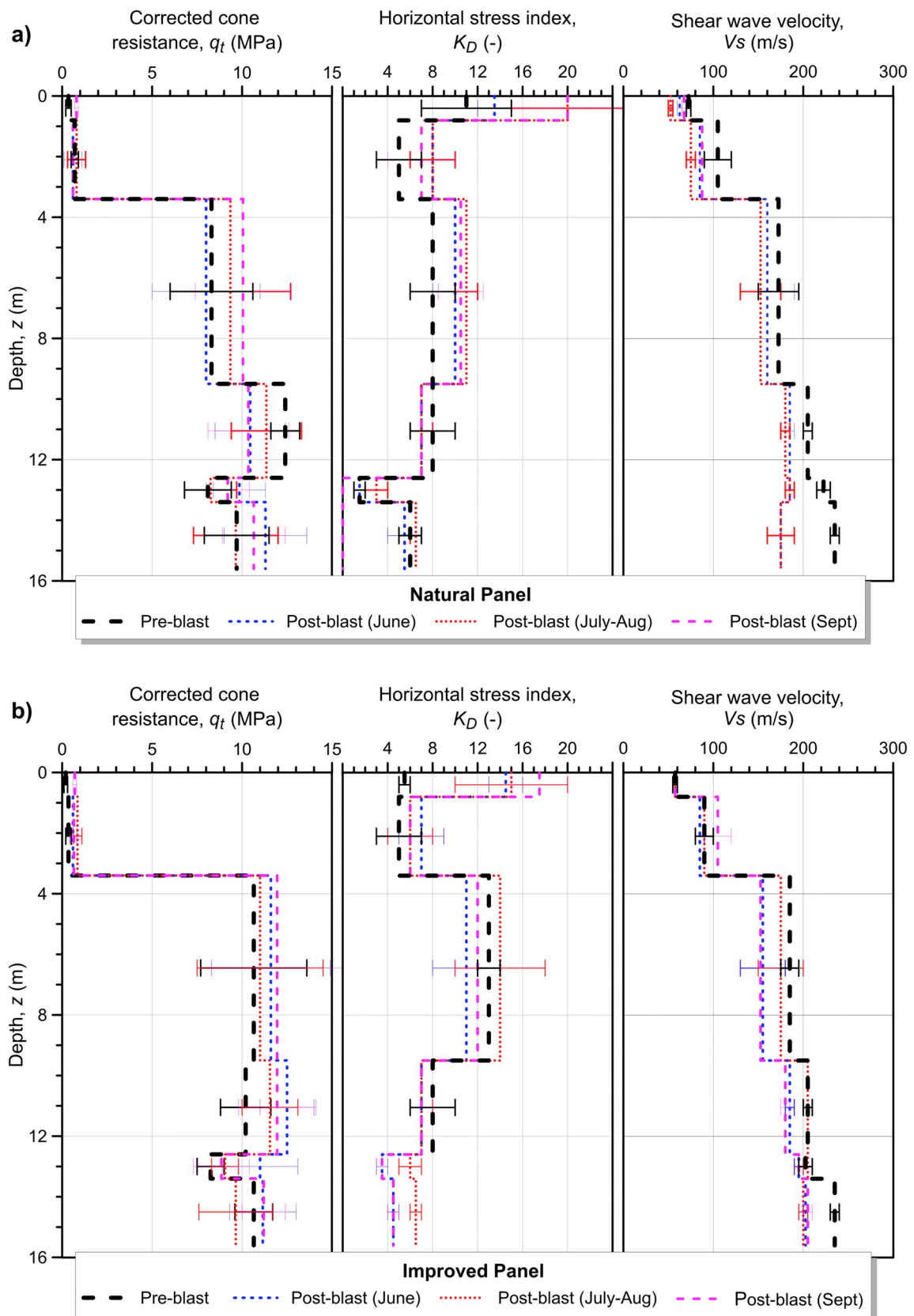


Fig. 11. Variation of the geotechnical and geophysical parameters before and after the blast test, obtained from CPTU and SDMT in the NP (a) and the IP (b).

effectiveness of the piers in silty sand deposits. On the other hand, a small increase is detectable for the same unit in NP (Fig. 11a), consistently with CPTU measurements, probably due to some densification

induced by the blast-liquefaction settlements. The bottom layers do not show any substantial increase. In later investigation campaigns, i.e. both in July–August and in September–October, K_D values stabilized in

both the blast areas, showing on average a significant increase only within the liquefiable layer in the IP.

Finally, post-blasting time-dependent stiffness changes cannot be clearly identified in the IP (Fig. 11b), while an overall small V_s decrease is observed in the NP (Fig. 11a). This last finding agrees, for example, with the results obtained by Mahvelati et al. (2016) in Pleistocene-aged sandy deposits, whereas differs from the observations made by Passeri et al. (2018) in Holocene-aged silty sands of Mirabello trial site (Emilia-Romagna, Italy). However, the Mirabello deposits are relatively new Holocene sands in comparison to the deposits of the present study area. Therefore, differences in geologic age and soil fabric may explain the differences in the rate and magnitude of stiffness changes.

In Fig. 12, the main results of the geoelectric surveys executed in the different time intervals in correspondence of the IP along the profile PS (see Fig. 2a, b, e, and f) are reported to a reliable investigation depth of 7 m. The measured resistivity data generally depict a very low resistivity environment (on average within 4–9 Ohm.m, Fig. 12a), even after the RAP construction (Fig. 12b). This is related both to the clayey and silty sand formations at the site and to the relevant saturating water conductivity. Indeed, water samples collected in wells located in the

area (Fig. 1) revealed anomalously high electrical conductivity values ($> 1200 \mu\text{S}/\text{cm}$). This condition, together with the low confining pressures due to pier installation near the ground surface, has influenced the imaged resistivity data, partially compromising the ability of the surveys in detecting resistivity changes related to the blast effects. Particularly, inverted resistivity data were not always able to image significant resistivity variations in the subsurface, particularly in the NP, contrary to previous literature examples (e.g. Passeri et al., 2018). For this reason, raw apparent resistivity data are presented only in the IP, since these data better reflect the local resistivity variations, particularly in correspondence with the RAP columns.

Indeed in the IP the comparison of resistivity distribution imaged before and after the RAP installation (Fig. 12a and b) satisfactorily defines the subsoil modifications related to the installation of the gravel columns (black dashed lines in Fig. 12b, c and d). The four RAPs intercepted by the survey line are indeed well depicted in the resistivity section showing a relatively higher resistivity with respect to the natural soil. The last column of the section is known to be driven only to 5.5 m depth. Nevertheless, apparent resistivity data also show a partial increase in resistivity at greater depths probably due to compaction of

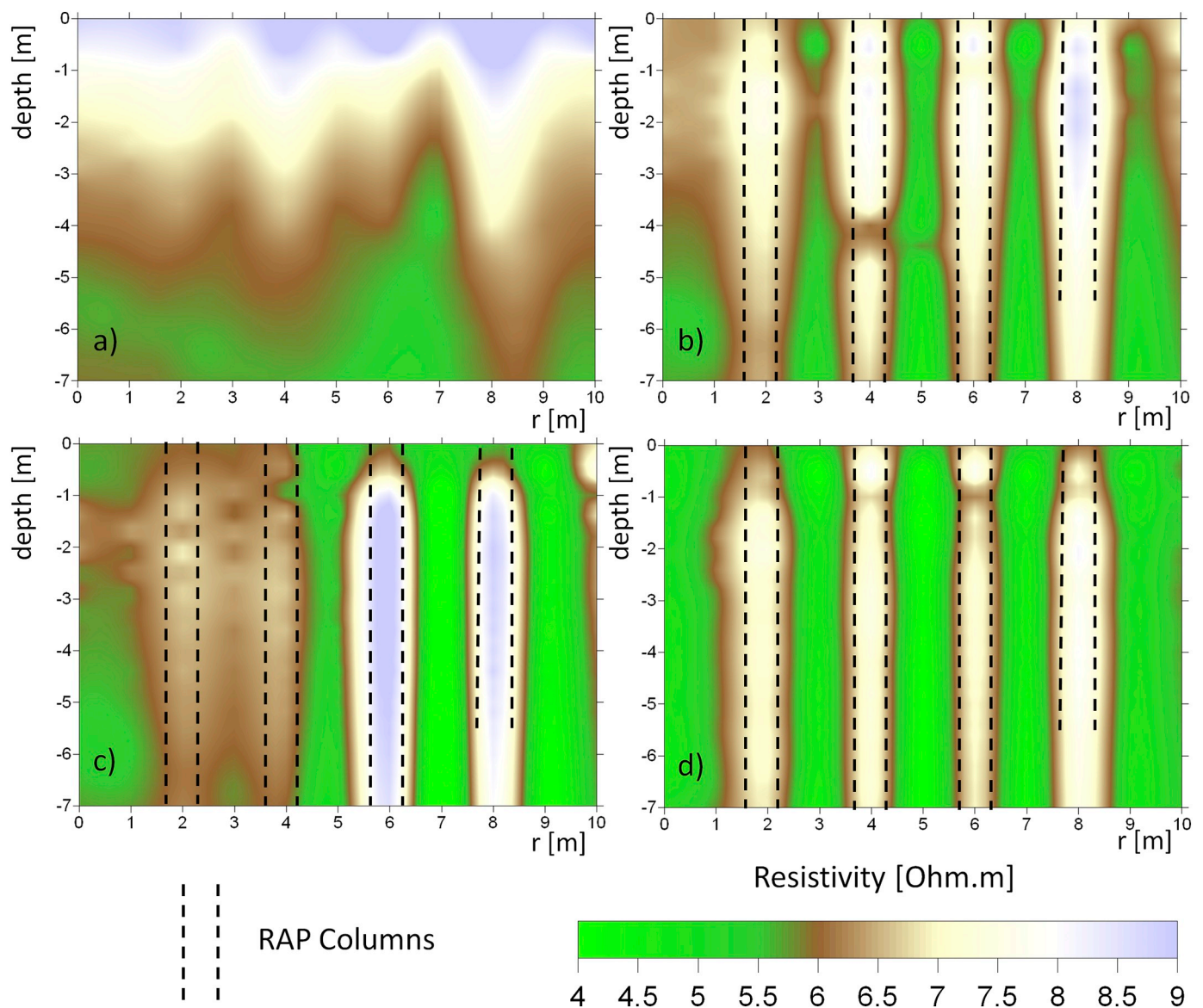


Fig. 12. Apparent resistivity data imaged along the profile PS in correspondence of the IP in the different time windows of the surveys: natural soil (a); treated soil before blast (b); treated soil after blast – June (c); treated soil after blast – September (d).

the subsoil following tamping. The first two piers along the section appear instead to be less homogeneous, as independently confirmed by quality control tests performed during their construction (Fig. 12b). After the blast testing the same first two piers along the section show a more significant resistivity reduction (Fig. 12c), which makes them less evident with respect to the surrounding soil. This effect could be related to increased water pressure in this zone of the IP and to partial column modifications after the blast which could have compromised RAP column resistance, given also their initial reduced stiffness. In this same zone of the IP, increased settlements after the blast have been depicted (Fig. 8) corroborating the geophysical evidence. Nevertheless, the apparent RAP column modifications do not appear to be permanent because the columns are again correctly imaged in the resistivity section acquired 4 months after the blast (Fig. 12d). Notwithstanding the difficult environment in terms of resistivity distribution, the geophysical surveys proved effective in imaging the variations induced by the blast tests within the RAP columns and can be suggested as a potential monitoring system.

Three trenches were excavated in the N350°-N355° direction (TR1a-c-d in Fig. 13a) and one in the transverse N65° direction (TR1b in Fig. 13a). The geometrical arrangement of the trenches made it possible to obtain detailed information on the sand boil genesis and on the previous fractures/conduits used by the liquefied sands in the 2012 earthquake. Particularly, the main sand boils developed during the blast tests shown in Fig. 6c reached the surface through the pore pressure transducer hole (PPT5, Fig. 13b and c). Evidence of liquefied sand ejected toward the surface was also found along the external part

of the profilometer (CNP, Fig. 13d). This sand was also observed filling a sub-horizontal fracture marking a stratigraphic contact (yellow flags in Fig. 13b) between a silty clay, with sparse pebbles and a few charcoals (stratigraphic level 1 in Fig. 13b), and an oxidized silty clay (stratigraphic level 2 in Fig. 13b and c). Evidence from the 2012 liquefaction (Fig. 13e and f) was also found in a 8 cm thick sand layer with a sharp basal contact on the vegetated surface at the time of the earthquake (Fig. 13e and f). The 2012 liquefied sand utilized an almost vertical thin fracture, visible to a depth of 1.5 m to reach the surface (Fig. 13g). A light grey clayey silt layer at the bottom of the trench (stratigraphic level 3 in Fig. 13c) was also observed, and provisionally recognized as one of the impermeable deposits over the liquefiable sand. The ejection of sand during the blast test largely utilized pre-existing artificial paths (PPT5 and CNP) and the weak stratigraphic contact between level 1 and 2.

6. Conclusions

Full-scale blast-induced liquefaction tests (Bondeno, Italy) made it possible to evaluate the effectiveness of Rammed Aggregate Pier® (RAP) treatment in mitigating liquefaction hazards in silty sands. A multi-disciplinary approach was used to increase the understanding obtained from the inter-related methods used to document blast-induced liquefaction behavior. The tests were performed on treated and untreated panels at a test site where sand boils indicated liquefaction during the 2012 M_w 6.1 Emilia-Romagna earthquake.

The controlled blasting experiment induced liquefaction in the

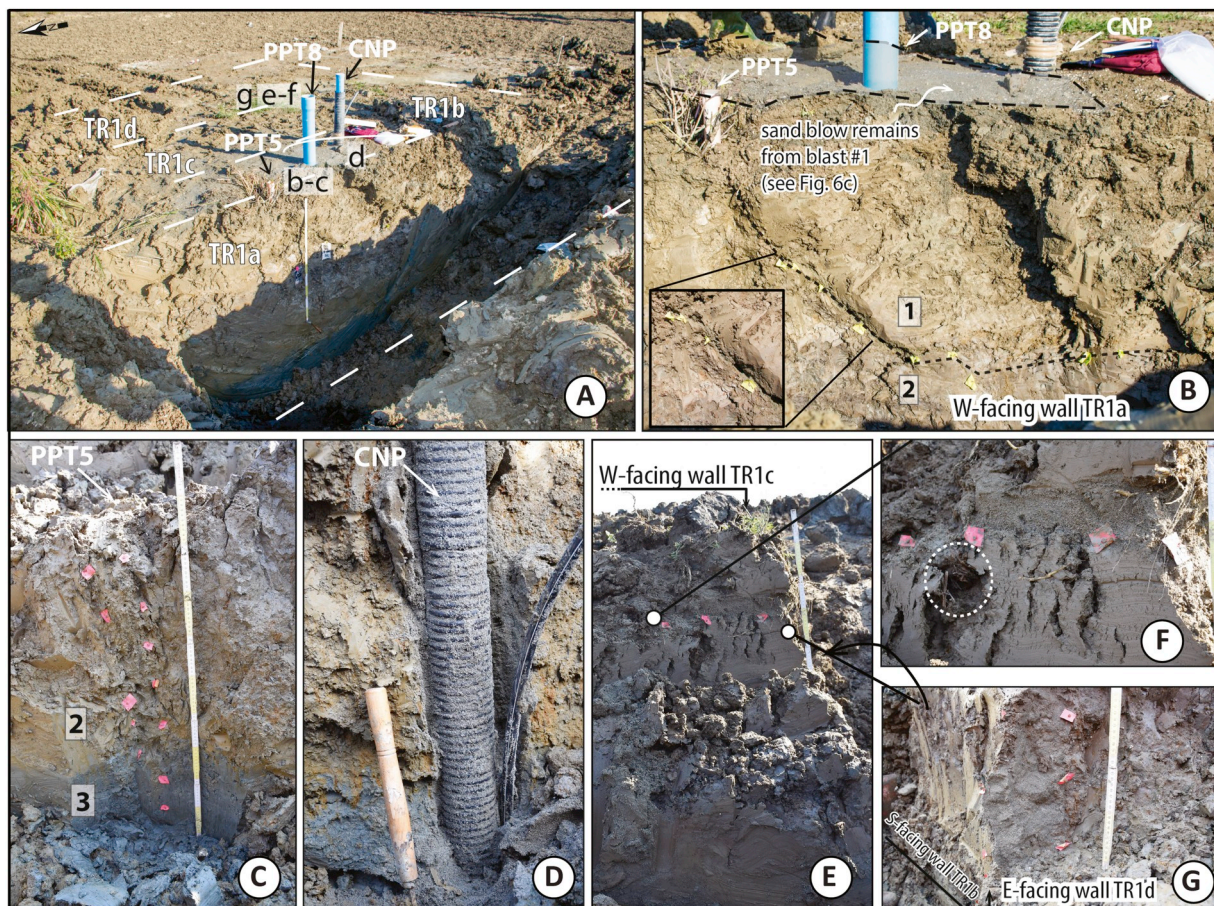


Fig. 13. Geometrical arrangement of the trenches (a); details of the most significant features exposed in the walls. Sand boils from the blast test (b) were generated by sand moving upward using the PPT5 pore pressure transducer, colored flags in (c), and the external part of the CNP profilometer (d) as conduits. Sand from CNP moved sub-horizontally, as shown by yellow flags, in (b). The white dashed circle in (f) indicates the remnants of the vegetation at the ground surface, covered by the 2012 sand blow (bottom of the blow marked by colored flags in e, f). Details of the 2012 vertical path (colored flags) developed along a thin fracture in (g). (For interpretation of the references to colour in this figure legend, the reader is referred to the web version of this article.)

natural panel (NP) consisting of untreated silty sands ($FC \approx 15\text{--}45\%$) and produced surface settlements of 7–10 cm. Numerous sand boils were induced and volumetric strains within the liquefied layers were similar to those that would be expected from earthquake-induced liquefaction, in agreement with previous blast experiments. Grain size distribution curves of the induced sand boils confirmed a selective loss of fines relative to the source beds in-situ (paleochannel of the Po River), in agreement with previous blast experiments and earthquake events. In-hole accelerometers were able to record maximum peak accelerations equal to 45 g and 52 g, and further analysis will be performed to estimate the blast-induced shear stress and shear strain.

Within the improved panel (IP), excess pore pressure ratios were lower than in the untreated panel, but still $> 75\%$. Despite these relatively high R_u values, the measured settlements (2–5 cm) were significantly lower than in the untreated natural panel, as confirmed by topographical surveys and geotechnical monitoring. In addition, sand boil formation was strongly reduced. Therefore, RAP treatment resulted in reducing liquefaction-induced settlements to acceptable levels for many structures in comparison with the untreated natural soil. The site investigations performed after blasting also confirmed that the treated soil maintains approximately its pre-blast geotechnical properties, while the natural untreated soil developed lower values that later recovered with time. After blasting, some temporary RAP modifications were also detected by the electrical resistivity profiles and topographical surveys in correspondence with the piers that showed lower stiffness during the construction procedure.

Further in-depth data analysis is necessary to understand the fundamental mechanisms leading to the reduction in settlement within the treated panel that may be related to soil densification, increased lateral stress, and composite soil-column behavior during reconsolidation.

Authors' contribution

The paper “Blast-induced liquefaction in silty sands for full-scale testing of ground improvement methods: insights from a multidisciplinary study”, by S. Amoroso, K.M. Rollins, P. Andersen, G. Gottardi, L. Tonni, M.F. García Martínez, K. Wissmann, L. Minarelli, C. Comina, D. Fontana, P.M. De Martini, P. Monaco, A. Pesci, V. Sapia, M. Vassallo, M. Anzidei, A. Carpena, F. Cinti, R. Civico, I. Coco, D. Conforti, F. Doumaz, F. Giannattasio, G. Di Giulio, S. Foti, F. Loddo, S. Lugli, M.R. Manuel, D. Marchetti, M. Mariotti, V. Materni, B. Metcalfe, G. Milana, D. Pantosti, A. Pesce, A.C. Salocchi, A. Smedile, M. Stefani, G. Tarabusi, G. Teza, describes the activities and the preliminary results of a multidisciplinary research that involved several different groups from Universities, Research Institutes and Companies with experience in the field of geology, geophysics, geotechnical engineering and topography. S. Amoroso and K.M. Rollins coordinated the research activities as Principal Investigators. All the authors contributed equally to the development of this research paper.

Declaration of competing interest

None.

Acknowledgements

The study was primarily funded by Geopier® Foundation Company (Davidson, North Carolina, United States). A special thanks also to Releo s.r.l. (Ferrara, Italy) who provided the installation of the Rammed Aggregate Piers free of charge. Financial contributions to this research activity were provided by INGV-FIRB Abruzzo project (“Indagini ad alta risoluzione per la stima della pericolosità e del rischio sismico nelle aree colpite dal terremoto del 6 aprile 2009”, <http://progettoabruzzo.rm.ingv.it/it>), by INGV-Abruzzo Region project (“Indagini di geologia, sismologia e geodesia per la mitigazione del rischio sismico”, L.R. n. 37/2016), by CIRI Edilizia e Costruzioni, University of Bologna, Italy

(TIRISICO PROJECT “Tecnologie Innovative per la riduzione del rischio sismico delle Costruzioni”, Project no. PG/2015/737636, POR-FESR 2014-2020), and by FAR UNIMORE 2018 “Sand liquefaction phenomena induced by seismic events: an interdisciplinary approach for assessing the liquefaction potential and improving resilience to earthquake-induced disasters”.

Special thanks to Brigham Young University for contributing to the realization of the blast test experiment in terms of personnel and technical equipment; to Scan&Go srl (Massimo Secchia) for the valuable help in TLS surveying by means of the Level Lift Roof -LP16R device for instrument installation; to Image SpA (Giorgio Amendolara) for data analysis and assistance in surveying operations; to the technicians from different Universities and Companies (Dave Anderson, Mario Marcolongo, Alessandro Lodi, Giovanni Bianchi, Gianni Petitti, Luigi Antonetti, Cristiano Prospero) that helped in the execution and elaboration of the geotechnical and geophysical tests.

A special thanks also to Michele Perboni who kindly guested the experimental activities, to the Bondeno Municipality (in particular Stefano Ansaloni, Olga Mantovani and Elena Bonora) and to the Emilia-Romagna Region (Luca Martelli), who provided all the necessary support to realize the research in collaboration with the other local authorities (Ferrara Prefecture, Ferrara Province, Local Civil Protection, Police).

The authors would also like to thank the anonymous reviewers for the valuable comments and suggestions to improve the article.

References

- Adalier, K., Elgamal, A., 2004. Mitigation of liquefaction and associated ground deformations by stone columns. *Eng. Geol.* 72, 275–291.
- Adalier, K., Elgamal, A., Meneses, J., Baez, J.I., 2003. Stone columns as liquefaction countermeasure in non-plastic silty soils. *Soil Dyn. Earthq. Eng.* 23, 571–584.
- Alexander, G., Arefi, J., Geoffrey, R.M., 2017. Performance of a stone column foundation system subjected to severe earthquake shaking. In: *Proceedings of the 3rd International Conference on Performance-based Design in Earthquake Geotechnical Engineering – PBD-III, Vancouver, Canada*.
- Amoroso, S., Milana, G., Rollins, K.M., Comina, C., Minarelli, L., Manuel, M.R., Monaco, P., Franceschini, M., Anzidei, M., Lusvardi, C., Cantore, L., Carpena, A., Casadei, S., Cinti, F.R., Civico, R., Cox, B.R., De Martini, P.M., Di Giulio, G., Di Naccio, D., Di Stefano, G., Facciorusso, J., Famiani, D., Fiorelli, F., Fontana, D., Foti, S., Madaia, C., Marangoni, V., Marchetti, D., Marchetti, S.L., Martelli, L., Mariotti, M., Muscolino, E., Pancaldi, D., Pantosti, D., Passeri, F., Pesci, A., Romeo, G., Sapia, V., Smedile, A., Stefani, M., Tarabusi, G., Teza, G., Vassallo, M., Villani, F., 2017. The first Italian blast-induced liquefaction test (Mirabello, Emilia-Romagna, Italy): description of the experiment and preliminary results. *Ann. Geophys.* 60 (5), S0556. <https://doi.org/10.4401/ag-7415>.
- Amoroso, S., Rollins, K.M., Monaco, P., Holtrigter, M., Thorp, A., 2018. Monitoring ground improvement using the seismic dilatometer in Christchurch, New Zealand. *Geotech. Test. J.* 41 (5), 946–966. <https://doi.org/10.1520/GTJ20170376>.
- Amoroso, S., Rollins, K.M., Andersen, P., Gottardi, G., Tonni, L., García Martínez, M.F., Wissmann, K., Minarelli, L., 2019. Full-scale testing of liquefaction mitigation using rammed aggregate piers in silty sands. In: *Proceedings of the 7th International Conference on Earthquake Geotechnical Engineering – 7 ICEGE, Rome, Italy*, pp. 656–663.
- Amoroso, S., Comina, C., Marchetti, D., 2020. Combined P- and S-wave measurements by seismic dilatometer test (SPDMT): a case history in Bondeno (Emilia Romagna, Italy). *Geotech. Test. J.* 43 (2). <https://doi.org/10.1520/GTJ20180233>.
- Ashford, S., Rollins, K.M., Lane, J., 2004. Blast-induced liquefaction for full-scale foundation testing. *J. Geotech. Geoenviron.* 130 (8), 798–806.
- ASTM D2487-11, 2011. Standard Practice for Classification of Soils for Engineering Purposes (Unified Soil Classification System). ASTM International, West Conshohocken, PA.
- Caputo, R., Poli, M.E., Minarelli, L., Rapti, D., Sboras, S., Stefani, M., Zanferrari, A., 2016. Palaeoseismological evidence for the 1570 Ferrara earthquake, Italy. *Tectonics* 35 (6), 1423–1445.
- Civico, R., Brunori, C.A., De Martini, P.M., Pucci, S., Cinti, F.R., Pantosti, D., 2015. Liquefaction susceptibility assessment in fluvial plains using airborne LIDAR: the case of the 2012 Emilia earthquake sequence area (Italy). *Nat. Hazards Earth Syst. Sci.* 15, 2473–2483.
- Cubrinovski, M., Bray, J.D., de la Torre, C., Olsen, M., Bradley, B., Chiaro, G., Stocks, E., Wotherspoon, L., Krall, T., 2018. Liquefaction-induced damage and CPT characterization of the reclamations at CentrePort, Wellington. *Bull. Seismol. Soc. Am.* 108 (3B), 1695–1708. <https://doi.org/10.1785/0120170246>.
- De Martini, P.M., Cinti, F.R., Cucci, L., Smedile, A., Pinzi, S., Brunori, C.A., Molisso, F., 2012. Sand volcanoes induced by the April 6th 2009 Mw 6.3 L'Aquila earthquake: a case study from the Fossa area. *Ital. J. Geosci.* 131, 410–422.
- Emergeo Working Group, 2013. Liquefaction phenomena associated with the Emilia

- earthquake sequence of May-June 2012 (Northern Italy). *Nat. Hazards Earth Syst. Sci.* 13 (4), 935–947.
- Finno, R.J., Gallant, A.P., Sabatini, P.J., 2016. Evaluating ground improvement after blast densification at the Oakridge landfill. *J. Geotech. Geoenviron.* 142 (1), 04015054.
- Fontana, D., Lugli, S., Marchetti Dori, S., Caputo, R., Stefani, M., 2015. Sedimentology and composition of sands injected during the seismic crisis of May 2012 (Emilia, Italy): clues for source layer identification and liquefaction regime. *Sediment. Geol.* 325, 158–167.
- Fontana, D., Amoroso, S., Minarelli, L., Stefani, M., 2019. Sand liquefaction phenomena induced by a blast test: new insights from composition and texture of sands (late Quaternary, Emilia, Italy). *J. Sediment. Res.* 89 (1), 13–27. <https://doi.org/10.2110/jsr.2019.1>.
- Gianella, T.N., Stuedlein, A., 2017. Performance of driven displacement pile-improved ground in controlled blasting field tests. *J. Geotech. Geoenviron.* 143 (9), 04017047.
- Giona Bucci, M., Villamor, P., Almond, P., Tuttle, M., Stringer, M., Ries, W., Smith, C., Hodge, M., Watson, M., 2018. Associations between sediment architecture and liquefaction susceptibility in fluvial settings: the 2010–2011 Canterbury Earthquake Sequence, New Zealand. *Eng. Geol.* 237, 181–197.
- Green, R.A., Olgon, C.J., Wissmann, K.J., 2008. Shear stress redistribution as a mechanism to mitigate the risk of liquefaction. In: *Proceedings of the 4th Geotechnical Earthquake Engineering and Soil Dynamics Conference: Liquefaction Triggering, Consequences, and Mitigation*, Sacramento, California, GSP 181.
- Harada, K., Orense, R.P., Ishihara, K., Mukai, J., 2010. Lateral stress effects on liquefaction resistance correlations. *Bull. N. Z. Soc. Earthq. Eng.* 43 (1), 13–23.
- Hwang, S., Roberts, J.N., Stokoe II, K.H., Cox, B.R., van Ballegooy, S., Soutar, C., 2017. Utilizing direct-push crosshole seismic testing to verify the effectiveness of shallow ground improvements: a case study involving low-mobility grout columns in Christchurch, New Zealand. In: *Proceedings of Grouting 2017*, Honolulu, Hawaii, pp. 415–424.
- Jamiolkowski, M., Lo Presti, D.C.F., Manassero, M., 2003. Evaluation of relative density and shear strength of sands from cone penetration test and flat dilatometer test. In: *Proceedings of Soil Behaviour and Soft Ground Construction*, GSP 119, pp. 201–238.
- Li, H., Liu, S., Tong, L., Xu, X., 2018. Investigating the resonant compaction effect on laterally loaded piles in layered soil. *Eng. Geol.* 246, 1–11.
- Luzi, L., Pacor, F., Ameri, G., Puglia, R., Burrato, P., Massa, M., Augliera, P., Franceschina, G., Lovati, S., Castro, R., 2013. Overview on the strong-motion data recorded during the May–June 2012 Emilia seismic sequence. *Seismol. Res. Lett.* 84 (4), 629–644.
- Mahvelati, S., Coe, J.T., Stuedlein, A.W., Asabere, P., Gianella, T.N., 2016. Time-rate variation of the shear wave velocity (site stiffness) following blast-induced liquefaction. In: *Proceedings of Proceedings of GeoChicago*, Chicago, Illinois, pp. 904–913.
- Marchetti, D., Monaco, P., Amoroso, S., Minarelli, L., 2019. In situ tests by Medusa DMT. In: *Proceedings of the XVII European Conference on Soil Mechanics and Geotechnical Engineering ECSMGE-2019*, Reykjavik, Iceland, <https://doi.org/10.32075/17ECSMGE-2019-0657>.
- Maurer, B.W., Green, R.A., Wotherspoon, L.M., Bastin, S., 2019. The stratigraphy of compound sand blows at sites of recurrent liquefaction: implications for paleoseismicity studies. *Earthquake Spectra* 35 (3), 1–20. <https://doi.org/10.1193/041818EQS097M>.
- Minarelli, L., Amoroso, S., Tarabusi, G., Stefani, M., Pulelli, G., 2016. Down-hole geophysical characterization of middle-upper Quaternary sequences in the Apennine Foredeep, Mirabello, Italy. *Ann. Geophys.* 59 (5), S0543. <https://doi.org/10.4401/ag-7114>.
- Mitchell, J.K., 2008. Mitigation of liquefaction potential in silty sands. In: *Proceedings of From Research to Practice in Geotechnical Engineering Congress 2008*, pp. 433–451.
- Mitchell, J.K., Solymer, Z.V., 1984. Time-dependent strength gain in freshly deposited or densified sand. *J. Geotech. Eng.* 110 (11), 1559–1576.
- Mitchell, J.K., Wentz, F.L., 1991. Performance of Improved Ground During the Loma Prieta Earthquake. Report No. UCB/EERC-91/12. University of California, Berkeley, CA.
- Molinari, I., Argnani, A., Morelli, A., Basini, P., 2015. Development and testing of a 3D seismic velocity model of the Po plain sedimentary basin, Italy. *Bull. Seismol. Soc. Am.* 105 (2A), 753–764.
- Narin van Court, W.A., Mitchell, J.K., 1994. Soil improvement by blasting. *J. Explos. Eng.* 12 (3), 34–41.
- Obermeier, S.F., 1998. Liquefaction evidence for strong earthquakes of Holocene and latest Pleistocene ages in the states of Indiana and Illinois, USA. *Eng. Geol.* 50, 227–254.
- Papathanassiou, G., Mantovani, A., Tarabusi, G., Rapti, D., Caputo, R., 2015. Assessment of liquefaction potential for two liquefaction prone areas considering the May 20, 2012 Emilia (Italy) earthquake. *Eng. Geol.* 189, 1–16.
- Passeri, F., Comina, C., Marangoni, V., Foti, S., Amoroso, S., 2018. Geophysical tests to monitor blast-induced liquefaction, the Mirabello (NE, Italy) test site. *J. Environ. Eng. Geophys.* 23 (3), 319–333. <https://doi.org/10.2113/JEEG23.3.319>.
- Pesci, A., Amoroso, S., Teza, G., Minarelli, L., 2018. Characterisation of soil deformation due to blast-induced liquefaction by UAV-based photogrammetry and terrestrial laser scanning. *Int. J. Remote Sens.* 39 (22), 8317–8336. <https://doi.org/10.1080/01431161.2018.1484960>.
- Pondrelli, S., Salimbeni, S., Perfetti, P., Danecek, P., 2012. Quick regional centroid moment tensor solutions for the Emilia 2012 (northern Italy) seismic sequence. *Ann. Geophys.* 55 (4), 615–621. <https://doi.org/10.4401/ag-6146>.
- Rayamajhi, D., Nguyen, T.V., Ashford, S.A., Boulanger, R.W., Lu, J., Elgamal, A., Shao, L., 2014. Numerical study of shear stress distribution for discrete columns in liquefiable soils. *J. Geotech. Geoenviron.* 140 (3), 04013034.
- Rayamajhi, D., Ashford, S.A., Boulanger, R.W., Elgamal, A., 2016. Dense granular columns in liquefiable ground. I: shear reinforcement and cyclic stress ratio reduction. *J. Geotech. Geoenviron.* 142 (7), 04016023.
- Robertson, P.K., Wride, C.E., 1998. Evaluating cyclic liquefaction potential using the cone penetration test. *Can. Geotech. J.* 35 (3), 442–459.
- Rollins, K.M., Lane, J.D., Nicholson, P.G., Rollins, R.E., 2004. Liquefaction hazard assessment using controlled blasting techniques. In: *Proceedings of 11th International Conference on Soil Dynamics and Earthquake Engineering*, Berkeley, California. 2. pp. 630–637.
- Saftner, D.A., Green, R.A., Hryciw, R.D., 2015. Use of explosives to investigate liquefaction resistance of aged sand deposits. *Eng. Geol.* 199, 140–147.
- Saftner, D.A., Zheng, J., Green, R.A., Hryciw, R., Wissmann, K., 2018. Rammed aggregate pier installation effect on soil properties. *Inst. Civil Eng.-Ground Improv.* 171 (2), 63–73.
- Salgado, R., Boulanger, R.W., Mitchell, J.K., 1997. Lateral stress effect on CPT liquefaction resistance correlations. *J. Geotech. Geoenviron.* 123 (8), 726–735.
- Smith, M.E., Wissmann, K., 2018. Ground improvement reinforcement mechanisms determined for the Mw 7.8 Muisne, Ecuador, earthquake. In: *Proceedings of the 5th Geotechnical Earthquake Engineering and Soil Dynamics Conference: Liquefaction Triggering, Consequences, and Mitigation – GEESDV 2018*, Austin, Texas, GSP 290, pp. 286–294.
- Stefani, S., Minarelli, L., Fontana, A., Hajdas, I., 2018. Regional deformation of late Quaternary fluvial sediments in the Apennines foreland basin (Emilia, Italy). *Int. J. Earth Sci.* 107 (7), 2433–2447. <https://doi.org/10.1007/s00531-018-1606-x>.
- Tonni, L., Gottardi, G., Amoroso, S., Bardotti, R., Bonzi, L., Chiaradonna, A., d’Onofrio, A., Fioravante, V., Ghinelli, A., Giretti, D., Lanzo, G., Madiati, C., Marchi, M., Martelli, L., Monaco, P., Porcino, D., Razzano, R., Rosselli, S., Severi, P., Silvestri, F., Simeoni, L., Vannucchi, G., Aversa, S., 2015. Interpreting the deformation phenomena triggered by the 2012 Emilia seismic sequence on the Canale Diversivo di Burana banks. *Riv. Ital. Geotecnica* 49 (2), 28–38. http://www.associazionegeotecnica.it/sites/default/files/rig/2_2015_028ton.pdf.
- Toscani, G., Burrato, P., Di Bucci, D., Seno, S., Valensise, G., 2009. Plio-Quaternary tectonic evolution of the northern Apennines thrust fronts (Bologna-Ferrara section, Italy): seismotectonic implications. *Ital. J. Geosci.* 128, 605–613.
- Vautherin, E., Lambert, C., Barry-Macaulay, D., Smith, M., 2017. Performance of rammed aggregate piers as a soil densification method in sandy and silty soils: experience from the Christchurch rebuild. In: *Proceedings of the 3rd International Conference on Performance-based Design in Earthquake Geotechnical Engineering – PBD-III*, Vancouver, Canada.
- Wentz, F.J., van Ballegooy, S., Rollins, K.M., Ashford, S.A., Olsen, M.J., 2015. Large scale testing of shallow ground improvements using blast-induced liquefaction. In: *Proceedings of the 6th International Conference on Earthquake Geotechnical Engineering – 6ICEGE*, Christchurch, New Zealand.
- Wissmann, K.J., van Ballegooy, S., Metcalfe, B.C., Dismuke, J.N., Anderson, C.K., 2015. Rammed aggregate pier ground improvement as liquefaction method in sandy and silty soils. In: *Proceedings of the 6th International Conference on Earthquake Geotechnical Engineering – 6ICEGE*, Christchurch, New Zealand.
- Wotherspoon, L.M., Cox, B.R., Stokoe II, K.H., Ashfield, D.J., Phillips, R.A., 2015. Utilizing direct-push crosshole testing to assess the effectiveness of soil stiffening caused by installation of stone columns and rammed aggregate piers. In: *Proceedings of the 6th International Conference on Earthquake Geotechnical Engineering – 6ICEGE*, Christchurch, New Zealand.
- Zhang, G., Robertson, P.K., Brachman, R.W.I., 2002. Estimating liquefaction-induced ground settlements from CPT for level ground. *Can. Geotech. J.* 39, 1168–1180. <https://doi.org/10.1139/T02-047>.